Neurons of the inferior olive respond to broad classes of sensory input while subject to homeostatic control

Homeostatic complex spike firing

Chiheng Ju[1,3], Laurens W.J. Bosman[1,3*], Tycho M. Hoogland[1,2,3*], Arthiha Velauthapillai[1], Pavithra Murugesan[1], Pascal Warnaar[1], Mario Negrello[1] and Chris I. De Zeeuw[1,2]

[1] Department of Neuroscience, Erasmus MC, 3015 GD Rotterdam, The Netherlands

[2] Netherlands Institute for Neuroscience, Royal Netherlands Academy of Arts and Sciences, 1105 BE Amsterdam, The Netherlands

[3] These authors contributed equally

* Correspondence to Dr. Laurens Bosman, PO Box 2040, 3000 CA Rotterdam, The Netherlands, l.bosman@erasmusmc.nl; or to Dr. Tycho Hoogland, PO Box 2040, 3000 CA Rotterdam, The Netherlands, t.hoogland@erasmusmc.nl

Keywords: cerebellum, inferior olive, homeostatic mechanisms, sensory integration, Purkinje cell, climbing fibre.

This article was first published as a preprint: Ju C, Bosman LWJ, Hoogland TM, Velauthapillai A, Murugesan P, Warnaar P, Negrello M & De Zeeuw CI. (2018). Neurons of the inferior olive respond to broad classes of sensory input while subject to homeostatic control. bioRxiv. https://doi.org/10.1101/379149

- **Purkinje cells in the cerebellum integrate input coming from the sensory organs with output generated by the motor control centres of the brain.**
- **Purkinje cells use sensory input to adapt motor control to the particularities of the direct surroundings of the animal.**
- **This study focused on one of the two main input pathways to Purkinje cells, the climbing fibres originating in the inferior olive, and asked whether they could convey mono- or multi-sensory information.**
- **We show that climbing fibres convey multiple types of sensory information and that they provide a mosaic projection pattern facilitating sensory integration in multiple combinations over the cerebellar cortex.**
- **Our results reveal that climbing fibres employ a coding pattern that underlies homeostatic control implying that their firing probability depends on their recent history of activity.**

Abstract

Cerebellar Purkinje cells integrate sensory information with motor efference copies to adapt movements to behavioural and environmental requirements. They produce complex spikes that are triggered by the activity of climbing fibres originating in neurons of the inferior olive. These complex spikes can shape the onset, amplitude and direction of movements and the adaptation of such movements to sensory feedback. Clusters of nearby inferior olive neurons project to "microzones" which are parasagitally aligned stripes of Purkinje cells. Although it is known that sensory input preferentially recruits coherent climbing fibre activity within one or more microzones, it is still unclear whether individual Purkinje cells within a single microzone integrate climbing fibre input from multiple distinct sources, or how sensory-evoked responses depend on the stimulus strength and recent history of climbing fibre activity. By imaging complex spike responses in cerebellar lobule crus 1 to various types of sensory stimulation in awake mice we find that different sensory modalities and receptive fields have a mild, but consistent, tendency to converge on individual Purkinje cells. Purkinje cells encoding the same stimulus show increased complex spike coherence and tend to lie close together. Moreover, whereas complex spike firing is only mildly affected by variations in stimulus strength, it strongly depends on the recent history of climbing fibre activity. Our data point towards a mechanism in the olivo-cerebellar system that regulates complex spike firing during mono- or multisensory stimulation around a relatively low set-point, highlighting an integrative coding scheme of complex spike firing under homeostatic control.

Introduction

The olivo-cerebellar system is paramount for sensorimotor integration during motor behaviour. The climbing fibres that originate in the inferior olive and cause complex spike firing in cerebellar Purkinje cells encode both unexpected and expected sensory events and affect initiation, execution as well as adaptation of movements (Albus, 1971; Welsh *et al.*, 1995; Kitazawa *et al.*, 1998; Gibson *et al.*, 2004; Bosman *et al.*, 2010; Yang & Lisberger, 2014; Ten Brinke *et al.*, 2015; Streng *et al.*, 2017; Apps *et al.*, 2018; Herzfeld *et al.*, 2018; Junker *et al.*, 2018; Romano *et al.*, 2018). Complex spike firing frequency is typically sustained around 1 Hz and not substantially affected by the behavioural state, although short-lived increases or decreases in firing occur (Bloedel & Ebner, 1984; Mukamel *et al.*, 2009; Bosman *et al.*, 2010; Zhou *et al.*, 2014; Hoogland *et al.*, 2015; Warnaar *et al.*, 2018). To date, the paradox between the persistence of complex spike firing and the behavioural relevance of individual complex spikes is still largely unresolved.

Whereas the afferents of Purkinje cells, including not only the climbing fibres but also the parallel fibres and axons of interneurons, all diverge, their efferents strongly converge upon the cerebellar nuclei, ultimately integrating many different inputs from the brain (Harvey & Napper, 1991; Sugihara *et al.*, 2001; Person & Raman, 2011). The parallel fibres are oriented in a transverse direction along the lobular axes, while the climbing fibres and axons of the interneurons are running perpendicularly to them in line with the sagittal orientation of the dendritic trees of Purkinje cells (Andersen *et al.*, 1964; Szentágothai, 1965; Sugihara *et al.*, 1999; Sullivan *et al.*, 2005; Gao *et al.*, 2006; Sugihara *et al.*, 2009; Ruigrok, 2011; Cerminara *et al.*, 2015; Apps *et al.*, 2018). Interestingly, the intrinsic biochemical nature as well as electrophysiological profile of individual Purkinje cells follows the organization of the climbing fibres so that Purkinje cells located in the same sagittal module receive climbing fibre input from the same olivary subnucleus and have similar identity properties, setting them apart from Purkinje cells in neighbouring modules (Xiao *et al.*, 2014; Zhou *et al.*, 2014; Cerminara *et al.*, 2015; De Zeeuw & Ten Brinke, 2015; Tsutsumi *et al.*, 2015; Suvrathan *et al.*, 2016). Accordingly, Purkinje cell responses following electrical stimulation of major nerves of cat limbs largely adhere to the parasagittal organization of the climbing fibre zones (Oscarsson, 1969; Groenewegen *et al.*, 1979), which in turn can be further differentiated into smaller microzones based upon their response pattern to tactile stimulation of a particular spot on the body (Ekerot *et al.*, 1991; Apps & Garwicz, 2005; Ozden *et al.*, 2009; De Zeeuw *et al.*, 2011). Possibly, differential sensory maps even occur at

the submicrozonal and individual Purkinje cell level, but this has to our knowledge not been investigated yet. In particular, it remains unclear to what extent different types of sensory inputs can drive complex spikes within the same individual Purkinje cells and/or their direct neighbours and how the strength as well as the history of these inputs influences the distribution of climbing fibre activity.

Here, we studied the impact of minimal stimuli of distinct sensory modalities on complex spike firing of Purkinje cells in crus 1 of awake mice using *in vivo* two-photon Ca^{2+} imaging. We found that different sensory streams appear to converge on individual inferior olivary neurons and thereby Purkinje cells, that sensory stimulation primarily affects the timing of the complex spikes rather than their rate, that the strength of complex spike responses varied seamlessly from non-responsive to highly responsive, that a recent history of high activity leads to a future of low activity, and that Purkinje cells that respond to the same stimulus tend to be located in each other's vicinity, increasing the coherence of their responses. Together, our data indicate that subtle and local sensory inputs can recruit mosaic ensembles of Purkinje cells, employing population coding in a spatially and temporally dynamic way that is in line with homeostatic control.

Methods

Ethical approval

All experimental procedures involving animals were in agreement with Dutch and European legislation and guidelines as well as with the ethical principles of The Journal of Physiology. The experiments were approved in advance by an independent ethical committee (DEC Consult, Soest, The Netherlands) as required by Dutch law and filed with approval numbers EMC2656, EMC3001 and EMC3168. Experiments were performed in compliance with the guidelines of the Animal Welfare Board of the Erasmus MC.

Animals and surgery

Mice were group housed until the day of the experiment and kept under a regime with 12 h light and 12 h dark with food and water available *ad libitum*. The mice had not been used for other experiments prior to the ones described here.

For the experiments performed in awake mice, we recorded from in total 66 field of views located in cerebellar lobule crus 1 of 29 male C57Bl/6J mice of 4-12 weeks of age (Charles Rivers, Leiden, The Netherlands). Prior to surgery, mice were anaesthetized using isoflurane (initial concentration: 4% V/V in O_2, maintenance concentration: ca. 2% V/V) and received Carprofen (Rimadyl, 5 mg/ml subcutaneously) to reduce post-surgical pain. Before the start of the surgery, the depth of anaesthesia was verified by the absence of a reaction to an ear pinch. To prevent dehydration, mice received 1 ml of saline s.c. injection before the surgeries commenced. Eyes were protected using eye ointment (Duratears, Alcon, Fort Worth, TX, USA). Body temperature was maintained using a heating pad in combination with a rectal thermometer. During surgery, we attached a metal head plate to the skull with dental cement (Superbond C&B, Sun Medical Co., Moriyama City, Japan) and made a craniotomy with a diameter of approximately 2 mm centred on the medial part of crus 1 ipsilateral to the side of somatosensory stimulation. The dura mater was preserved and the surface of the cerebellar cortex was cleaned with extracellular solution composed of (in mM) 150 NaCl, 2.5 KCl, 2 $CaCl_2$, 1 $MgCl_2$ and 10 HEPES (pH 7.4, adjusted with NaOH). After the surgery, the mice were allowed to recover from anaesthesia for at least 30 minutes. Subsequently, the mice were head-fixed in the recording setup and they received a bolus-loading of the Ca^{2+} indicator Cal-520 (0.2 mM; AAT Bioquest, Sunnyvale, CA) (Tada *et al.*, 2014). The dye was first dissolved with 10% w/V Pluronic F-127 in DMSO (Invitrogen, Thermo Fisher Scientific, Waltham, MA, USA) and then diluted 20 times in the extracellular solution. The dye solution

was pressure injected into the molecular layer (50–80 μm below the surface) at 0.35 bar for 5 min. Finally, the brain surface was covered with 2% agarose dissolved in saline (0.9% NaCl) in order to reduce motion artefacts and prevent dehydration.

For the experiments on single-whisker stimulation we made recordings under anaesthesia on 17 male C57BL/6J mice of 4-12 weeks of age. The procedure was largely the same as described above, but instead of isoflurane we used ketamine/xylazine as anaesthetic (i.p. injection via butterfly needle, initial dose: 100 mg/kg and 10 mg/kg, respectively; maintenance dose: approximately 60 mg/kg/h and 3 mg/kg/h, respectively). The mice remained under anaesthesia until the end of the recording. A subset of these experiments was performed with 0.2 mM Oregon Green BAPTA-1 AM dye (Invitrogen) as this dye has been more widely used than Cal-520 (e.g., (Stosiek *et al.*, 2003; Ozden *et al.*, 2009; Schultz *et al.*, 2009; Hoogland *et al.*, 2015). Oregon Green BAPTA-1 AM was dissolved and applied in the same way as Cal-520. We found that Cal-520 had a superior signal-to-noise ratio under our experimental conditions. As a consequence, the observed event rate was lower in the experiments using OGB-1 (OGB-1: 0.45 ± 0.26 Hz; n = 172 cells; Cal-520: 0.72 ± 0.40 Hz; n = 43 cells; median ± IQR; U = 1719.0, $p < 0.001$, Mann-Whitney test). The observed frequency range using Cal-520 was comparable to that found using *in vivo* single-unit recordings under ketamine/xylazine anaesthesia: 0.6 ± 0.1 Hz (Bosman *et al.*, 2010). Despite an underestimation of the complex spike rate using OGB-1, we found that the ratios of Purkinje cells that responded to single whisker stimulation were similar for both dyes (OGB-1: 89 out of 373 cells (24%); Cal-520: 35 out of 152 cells (23%); $p = 0.910$; Fisher's exact test). For this reason, we combined the data from both dyes. For the analysis presented in Fig. 7, we included only those cells that could be recorded during all stimulus conditions. All experiments using awake data were obtained with Cal-520.

At the end of each experiment, the mice were killed by cervical dislocation under isoflurane or ketamine/xylazine anaesthesia after which the brain was removed and the location of the dye injection in crus 1 was verified by epi-fluorescent imaging.

In vivo *two-photon Ca^{2+} imaging*

Starting at least 30 min after dye injection, *in vivo* two-photon Ca^{2+} imaging was performed of the molecular layer of crus 1 using a setup consisting of a Ti:Sapphire laser (Chameleon Ultra, Coherent, Santa Clara, CA, USA), a TriM Scope II system (LaVisionBioTec, Bielefeld, Germany) mounted on a BX51 microscope with a 20x 1.0 NA water immersion objective (Olympus, Tokyo, Japan) and GaAsP photomultiplier detectors (Hamamatsu, Iwata City,

Japan). A typical recording sampled a field of view of 40 x 200 µm with a frame rate of approximately 25 Hz.

Sensory stimulation

Cutaneous stimuli were delivered to four defined regions on the left side of the face, ipsilateral to side of the craniotomy. These regions were the whisker pad, the cheek posterior to the whisker pad, the upper lip and the lower lip. Stimuli were applied using a Von Frey filament (Touch Test Sensory Evaluator 2.83, Stoelting Co., IL, USA) attached to a piezo linear drive (M-663, Physik Instrumente, Karlsruhe, Germany). Prior to the set of experiments described here, we tested a series of 8 Von Frey filaments with a stiffness range from 0.02 g to 1.4 g in awake head-fixed mice to select the optimal force for these experiments. We selected the 0.07 g (0.686 mN) filament because this filament induced a mild reaction in the mouse, but no signs of a nociceptive response (cf. Chaplan *et al.* (1994)). The touch time was fixed at 100 ms. As a control, we moved the stimulator without touching the face ("sound only" condition). Visual stimuli were delivered as 10 ms pulses using a 460 nm LED (L-7104QBC-D, Kingbright, CA, USA). The stimulation frequency was fixed at 1 Hz and the different stimuli were applied in a random order. Video-recordings of the eye, made under infrared illumination, revealed that the mice did not make eye movements in response to the LED flash, but they did show reflexive pupil constriction (*data not shown*).

Single whiskers were stimulated using a piezo linear drive (M-663, Physik Instrumente) while using a deflection of 6°. It took the stimulator approximately 30 ms to reach this position. At the extreme position, the stimulator was paused for 150 ms before returning to the neutral position. The stimulator was designed to minimize contact with other whiskers. Each stimulation experiment consisted of five sessions in random order. During each block one of the ipsilateral whiskers B2, C1, C2, C3 and D2 was stimulated. Each session consisted of 150 stimuli at 2 or 3 Hz.

Complex spike detection

Image analysis was performed offline using custom made software as described and validated previously (Ozden *et al.*, 2008; Ozden *et al.*, 2012; De Gruijl *et al.*, 2014). In short, independent component analysis was applied to the image stack to discover masks describing the locations of individual Purkinje cell dendrites (e.g., see Fig. 2A). For each field of view the mask was generated only once, so that the same Purkinje cells were analysed for subsequent recordings of different stimulus conditions enabling paired comparisons.

Experiments during which spatial drift occurred were discarded from subsequent analysis. The fluorescence values of all pixels in each mask were averaged per frame. An 8% rolling baseline from a time window of 0.5 ms was subtracted from the average fluorescence per mask (Ozden et al. 2012), after which Ca^{2+} transient events were detected using template matching

Statistical analysis

In general, we first tested whether parameter values were distributed normally using one-sample Kolmogorov-Smirnov or Shapiro-Wilk tests. If not, non-parametric tests were applied. When multiple tests were used, Benjamini-Hochberg correction for multiple comparisons was applied. For each experiment, stimuli were given in a random sequence. Identification of Purkinje cell dendrites and event extraction were performed by a researcher who was blind to the type of stimulus. For the experiments characterizing response characteristics of individual Purkinje cells, we compared the fraction of responsive Purkinje cells, the response latency and the response peak. After extracting the Ca^{2+} transient event times, peri-stimulus time histograms (PSTHs) were constructed using the inter-frame time (approx. 40 ms) as bin size. Stacked line plots of Purkinje cell PSTHs were sorted by weak to strong peak responses. The data were normalized such that the top represents the average responses of all Purkinje cells. Statistical significance of responses occurring within 200 ms from stimulus onset was evaluated using a threshold of the mean + 3 s.d. of the firing rate during the 500 ms prior to stimulus onset (300 ms for the single whisker stimulation experiments, as they were performed with a higher stimulation frequency).

To calculate whether two or more inputs converged on single Purkinje cells we used a bootstrap method. First, we determined the fraction of responsive cells for each parameter and compared these to a randomly generated number between 0 and 1 as taken from a uniform distribution. If for each input the randomly generated numbers were lower than the measured fractions, we considered them as responsive to all stimuli. This procedure was repeated 10,000 times and the average and standard deviation were derived and used to calculate the *Z* score of the experimental data. All bootstrap procedures were performed using custom-written code in LabVIEW (National Instruments, Austin, TX, USA).

The distributions of pairs of Purkinje cells, either both responsive to a given stimulus ("responsive pairs") or one cell being responsive and the other not ("heterogeneous pairs"), were tested using two-dimensional Kolmogorov-Smirnov tests performed in MATLAB (MathWorks, Natick, MA, USA). Aggregate PSTHs (Fig. 9) were constructed and evaluated

as described before (Romano *et al.*, 2018). Briefly, we calculated per individual frame the number of simultaneously occurring events and colour coded these in a PSTH combining data from all dendrites in a field of view. Based upon the total number of complex spikes and dendrites per recording, we calculated the expected number of simultaneous complex spikes per individual frame based upon a Poisson distribution. The actual number of simultaneous complex spikes was compared to this calculated distribution and a *p* value was derived for each number based upon the Poisson distribution (using custom-written software in MATLAB and LabVIEW). Correlation analysis was performed in SigmaPlot (Systat Software, San Jose, CA, USA) and, unless mentioned otherwise, the rest of the statistical tests were performed using SPSS (IBM, Armonk, NY, USA).

Results

Climbing fibre responses to tactile, auditory and/or visual input

Little is known about the distribution and convergence of different types of climbing fibre-mediated sensory input at the level of individual, nearby Purkinje cells. Here, we performed two-photon Ca^{2+} imaging of Purkinje cells of awake mice to record complex spikes responses to various types of sensory stimulation related to the face of the mice. The recordings were made in crus 1 as this lobule is known to receive sensory input from the oro-facial region (Fig. 1A) (Shambes *et al.*, 1978; De Zeeuw *et al.*, 1990; Yatim *et al.*, 1996; Apps & Hawkes, 2009; Bosman *et al.*, 2011; De Gruijl *et al.*, 2013; Kubo *et al.*, 2018). The configurations and positions of individual Purkinje cell dendrites were detected using independent component analysis (Fig. 1B). Ca^{2+} transients were isolated per dendrite by a template-matching procedure that reliably detects complex spikes (Ozden *et al.*, 2008; Najafi & Medina, 2013; De Gruijl *et al.*, 2014) (Fig. 1C-E).

We started our study of sensory responses by using air puff stimulation of the large facial whiskers, which is a relatively strong stimulus. In line with previous studies (Axelrad & Crepel, 1977; Brown & Bower, 2002; Bosman *et al.*, 2010; Apps *et al.*, 2018; Romano *et al.*, 2018), we found that air puff stimulation to the whiskers evoked complex spike responses in many Purkinje cells (e.g., in 19 out of 19 Purkinje cells in the example illustrated in Fig. 2). In total, 102 out of the 117 (87%) cells analysed were considered to be responsive to such a stimulus, implying that the peak responses of these cells exceeded the threshold of the average + 3 s.d. of the pre-stimulus period.

To address whether localized and more subtle stimuli recruited smaller groups of Purkinje cells, maybe even subsets of microzones, we subsequently applied gentle tactile stimulation at four facial locations: the whisker pad, the cheek posterior to the whisker pad, the upper lip and the lower lip (Fig. 3A). The stimuli were given using a Von Frey filament (target force = 0.686 mN) attached to a piezo actuator. The stimulus strength was carefully calibrated to avoid inducing responses from neighbouring skin areas or nociceptive responses (see Methods). When we evaluated the strength of the Purkinje cell responses to any of the four tactile stimuli (998 stimulus conditions in 282 Purkinje cells), a skewed, but continuous distribution was found (Fig. 3B). Moreover, also for individual stimulus locations skewed, but continuous distributions of response strengths were found, with the upper lip being the least sensitive of the four facial areas (Fig. S2). In other words, our data set contained Purkinje cells that did not respond at all as well as cells that responded strongly, with all gradients in

between. Thus, a distinction between "responsive" and "non-responsive" Purkinje cells involved a somewhat arbitrary distinction, prompting us to present most of the subsequent analyses using the entire dataset.

Given that the touches were delivered by a piezo-actuator that made a weak but audible sound, we also tested whether Purkinje cells responded to this sound in the absence of touch. This was the case, and, as expected, the "sound-only" stimulus evoked the weakest responses of all stimuli ($p < 0.001$; Kruskal-Wallis test; Fig. S2B). For comparison, we also included a visual stimulation, consisting of a brief flash of a blue LED. This stimulus evoked responses with a similar strength as the whisker pad and lower lip stimulation, but with a latency that was remarkably long (Fig. S2A).

To facilitate a quantitative comparison between the stimulus conditions, we subsequently focused on the subset of obvious responses, defined as having a peak amplitude exceeding our threshold for significance set at the average + 3 s.d. of the pre-stimulus period. Among these "significantly responding" Purkinje cells, we found trends as in the entire population: the lower lip recruited the strongest responses, directly followed by the whisker pad and visual stimulation, while upper lip and sound-only stimulations were less effective (Fig. 3C-E; Table 1). We also confirmed the remarkably long latency, typically more than 100 ms, for the visually evoked responses ($p < 0.001$ compared to the tactile stimuli; Kruskal Wallis test; Fig. 3F; Table 1).

Convergence of sensory inputs

Next, we addressed the question whether Purkinje cells have a preference to respond to one or multiple types of stimulation. To this end, we made for each combination of two stimuli a scatter plot of the response strengths of each individual Purkinje cell. For each and every combination, correlation regression analysis revealed a positive correlation, implying that a stronger response to one stimulus typically implied also a stronger response to the other (Fig. 4A). These correlations, although weak, were statistically significant for all combinations except in two cases (i.e., upper lip vs. sound only and upper lip vs. visual stimulation; Table 2). The regression lines deviated from the 45° line, suggesting that, although there is a tendency at the population level to combine inputs, individual Purkinje cells can display specificity for a given stimulus. The Venn diagrams in Fig. 4B-C highlight the degree of overlap for all combinations of two and three stimuli. For all combinations we found some but no complete overlap. Remarkably, when comparing the observed overlap with the expected overlap based upon a random distribution, all combinations occurred more often than

predicted. We performed a bootstrap analysis (see Methods) to infer statistical significance and indeed, most combinations were observed significantly more often than expected from a random distribution of inputs (Fig. 4B-C, Tables 3 and 4). This also included the visual stimulation, so that those Purkinje cells responding to a tactile stimulus typically were responsive to visual stimulation as well.

With an apparent lack of input-specificity, one might wonder whether Purkinje cells in crus 1 are encoding specific sensory events or, alternatively, respond indifferently to any external trigger. In this respect, especially the response pattern to the sound only stimulus is noticeable. A weak, but audible sound was generated by the piezo actuator used to deliver the tactile stimuli. Hence, all tactile stimuli also involved sound. Nevertheless, the Venn diagrams in Fig. 4B show that there are Purkinje cells that responded statistically significantly to sound only, but not to sound and touch delivered simultaneously. This could be taken as an argument against the input-specificity of Purkinje cells. However, one should keep in mind that the separation between "responsive" and "non-responsive" Purkinje cells is arbitrarily (cf. Fig. 3B), and to be able to draw such a conclusion, there should be a consistent absence of preferred responses. The sound only stimulus was found to be the weakest stimulus (Figs. 3E and S2B) and pair-wise comparisons of the response strengths had a strong bias towards the stimuli involving touch (Fig. 4A). This is further illustrated in a single experiment, directly comparing the responses evoked by whisker pad touch and sound only stimulation. Four randomly selected Purkinje cells from this experiment failed to show a response to sound only stimuli in the absence of touch responses (Fig. S3A-E). This was confirmed by the group-wise analysis of all Purkinje cells in this experiment, demonstrating a clear preference for the whisker pad stimulation over the sound-only stimulus (Fig. S3F-G). Overall we conclude that, although the observed responses to mild sensory stimulation are typically weak and convergent, a certain degree of input-specificity was observed in Purkinje cells of crus 1.

Stimulus strength has limited impact on complex spike responses

To avoid recruiting responses from adjacent areas, we used weak stimulation strengths (Figs. 3 and 4). Under anaesthesia, the strength of a stimulus affects the complex spike response probability (Eccles *et al.*, 1972; Bosman *et al.*, 2010). This finding has been reproduced in awake mice using variations in duration and strength of peri-ocular air puff stimulation (Najafi *et al.*, 2014). As a consequence, our approach using weak stimuli could have led to an underestimation of the number and spatial extent of sensory climbing fibre responses. To study whether the stimulus strength could also have affected our results, we performed an

299 experiment in which we stimulated all whiskers mechanically with three different strengths,
300 the largest of which was identical to the maximal stimulus we previously applied under
301 anaesthesia (Bosman *et al.*, 2010). The chosen stimulus intensities maximized the variation in
302 kinetic energy, which was the most salient feature for barrel cortex neurons (Arabzadeh *et al.*,
303 2004). Stimuli were randomly intermingled (Fig. 5A-B). Raw traces indicate that, even at the
304 ensemble level, (relatively) weak stimuli do not trigger responses at every trial and
305 spontaneous complex spike firing may occasionally appear as peaks prior to stimulus onset
306 (Figs. 2C, 5C and 5D).
307 Of the 340 Purkinje cells tested in awake mice, 209 (61%) responded significantly to
308 at least one stimulus strength. In these 209 Purkinje cells, we compared the complex spike
309 responses across three intensities. The weak and the moderate intensities (1 mm displacement
310 reached in 62 ms and 2 mm displacement reached in 31 ms, respectively) showed a
311 comparable number of responses and only the strong stimulus intensity (4 mm reached in 16
312 ms) evoked significantly more responses ($F(2) = 57.160$, $p < 0.001$, Friedman's test) (Figs.
313 5D-F, S4A). Despite being 16 times faster (250 mm/s instead of 16 mm/s), the strongest
314 stimulus recruited only 28% (measured as peak response) or 34% (measured as integral of
315 whole response period) more complex spikes than the weak stimulus (Fig. 5E-F). The same
316 analysis on the whole population of Purkinje cells, including those that did not show a
317 statistically significant response, revealed even less of an impact of stimulus strength (Fig.
318 S4B). We therefore conclude that the complex spike response poorly encodes velocity of
319 whisker displacement in awake mice and that – within boundaries – using stronger stimuli
320 does not necessarily lead to qualitatively different results.
321
322 *Functionally equivalent Purkinje cells tend to group together*
323 So far, we mainly found an abundance of weak and not very specific complex spike responses
324 to mild sensory stimulation. One way in which such weak responses at the cellular level could
325 still have considerable effects on the network level would be when functionally equivalent
326 Purkinje cells would lie together in microzones. Indeed, as the Purkinje cells of each
327 microzone project to a group of adjacent neurons in the cerebellar nuclei (Voogd &
328 Glickstein, 1998; Apps & Hawkes, 2009), population encoding of sensory events may be a
329 form of functional signalling in the olivo-cerebellar system. Fig. 6 illustrates to what extent
330 adjacent Purkinje cells have similar stimulus response probabilities. In this example, Purkinje
331 cells reacting strongly to whisker pad stimulation are grouped together, but such a spatial
332 clustering does not seem to be perfect, as also a few strongly responsive cells are located in

between less responsive Purkinje cells (Fig. 6A) and as upper lip-responsive Purkinje cells are sparsely distributed across the same area (Fig. 6B). We reasoned that spatial clustering should imply that two neighbouring cells have more similar response probabilities than randomly selected cells from the same field of view. This turned out to be the case, but only if we confined our focus to Purkinje cells with statistically significant responses ($Z > 3$) (Figs. 6C and 6D). Thus, especially the Purkinje cells with stronger responses to a given stimulus type were found to be located more closely together than could be expected from a random distribution.

Single whisker responses in Purkinje cells

Using our tactile stimuli we demonstrated a tendency of nearby Purkinje cells to encode the same stimulus. To study whether this would hold true for even smaller receptive fields we turned to single whisker stimulation. Using single-unit electrophysiological recordings we have previously shown that stimulation of a single whisker is sufficient to evoke complex spike responses (Bosman *et al.*, 2010). Individual whiskers can be reliably identified across mice and as such they can be qualified as minimal reproducible receptive fields. We repeated our previous single-whisker stimulation experiments now using two-photon Ca^{2+} imaging focusing on five whiskers that were stimulated individually in a random sequence. To prevent spontaneous whisking and thereby interference by other whiskers, these experiments were (unlike all other experiments in this study) performed under anaesthesia. In general, the responses were specific, as many Purkinje cells responded to a particular whisker, but not to its neighbouring whiskers (Fig. 7A). Overall, of the 148 Purkinje cells tested, 31 (21%) responded significantly to only one of the five whiskers tested, 14 (10%) to two and 5 (3%) to three whiskers (Fig. 7B). Not all whiskers were equally effective in recruiting Purkinje cell responses: 23 cells (15%) responded significantly to C3 stimulation, but only 4 (3%) to C1 stimulation. Likewise, pairs of more anterior whiskers had higher chances to be encoded by the same Purkinje cell (Fig. 7C; Table 5). Thus, also for single whisker stimulation, there was a balance between sensory integration and specificity.

Next, we examined the spatial distribution of responsive Purkinje cells. In Fig. 7D two nearby recording spots from the same mouse are shown. In recording spot 1, from which the example in Fig. 7A originates, all Purkinje cells responded to stimulation of at least one whisker. However, in the second recording spot, only two Purkinje cells responded: both to a single, but different whisker. For each recording spot we compared responsive vs. non-responsive Purkinje cells, taking the average + 3 s.d. of the baseline as threshold for

responsiveness. This yielded a clear separation for the Purkinje cells in the first, but a rather poor one in the second recording spot (Fig. 7E). In terms of number of responsive Purkinje cells and response amplitudes, these two recordings, although made from the same lobule in the same animal, form relatively extreme examples in our dataset. When plotting the response strength versus the fraction of responsive Purkinje cells per field of view, we found a positive correlation (Pearson correlation: R = 0.5208; $p < 0.001$; Fig. 7F), implying that Purkinje cells with stronger responses to a certain whisker tended to be surrounded by other Purkinje cells encoding the same whisker – in line with the much stronger responses in the first than in the second recording spot illustrated in Fig. 7D-E. Taken together, stimulating single whiskers revealed a similar organization as did the less specific stimuli (see Fig. 6) with a clear tendency of Purkinje cells with the same receptive field to be located close together. However, the spatial clustering was incomplete and especially weakly responsive Purkinje cells were found to be interspersed with completely unresponsive Purkinje cells.

Functionally equivalent Purkinje cells fire coherently

In addition to spatial clustering, a second requirement for population encoding is coherence of complex spike firing. As coherence can be affected by anaesthesia, we applied our coherence analysis on spontaneous and modulation data obtained from Purkinje cells with significant responses in awake mice. We defined coherence as firing within the same frame of 40 ms, which still falls well within the subthreshold oscillation cycle of inferior olivary neurons *in vivo* (Khosrovani *et al.*, 2007). Pairs of Purkinje cells with significant responses upon whisker pad stimulation showed a significantly increased level of coherence ($p < 0.001$; two-dimensional Kolmogorov-Smirnov test) compared to that of heterogeneous pairs (i.e. pairs of one responsive and one non-responsive Purkinje cell) (Fig. 8A-B). When we examined the firing pattern of the same pairs in the absence of sensory stimulation, we found similar results (Fig, 8C), indicating that it is not the sensory input per se that directs coherence. These findings were confirmed in the whole population, taking also the other tactile and visual stimuli into account (Fig. 8D-E). Only stimulation of upper lip, the area least represented among the recorded Purkinje cells (Fig. 3), revealed less of a discrimination between significantly responsive and heterogeneous pairs. Hence, we conclude that not only spatial clustering but also coherence patterning of functionally equivalent Purkinje cells may facilitate population encoding.

Population responses

Although we found increased coherent firing in functionally equivalent Purkinje cells, the level of coherence was still relatively low, with a regression coefficient seldom exceeding 0.3 (Fig. 8). However, in this analysis we did not discriminate between complex spikes firing in response to sensory stimulation and complex spikes occurring spontaneously. Therefore, we subsequently quantified the distribution of complex spikes over time. This is illustrated for a representative field of view in Fig. 9A. For each frame, we summed all complex spikes of the 17 Purkinje cells in this field of view and subsequently made an aggregate peri-stimulus time histogram of all these Purkinje cells, whereby we colour-coded the number of complex spike recorded per frame (see also Romano *et al*. (2018)).. The darker the colour, the more complex spikes occurred simultaneously. Clearly, the darker colours – and thus the stronger coherence – were observed during the stimulus response period. This occurrence of coherent firing over time was compared with a random redistribution of the spikes per Purkinje cell (based upon a Poisson distribution). Note that an equal distribution would imply on average less than two complex spikes being fired during each frame, indicating the highly patterned distribution found during the experiments. The grey bars in Fig. 9B indicate the level of coherence that could be expected by chance, while the red ones indicate highly unlikely values. This shows that especially the higher levels of coherence are task-related, while spatially isolated firing occurs irrespective of stimulation.

Examination of the aggregate PSTHs confirms what could already be seen in Fig. 3D, in that there is a trend of reduced inter-trial firing for those stimuli with a relatively strong response (Fig. 9). In this experiment, we plotted the responses to air puff stimulation, which recruited statistically significant responses in 17 out of 17 Purkinje cells, on top of those to lower lip stimulation, which recruited only 1 of the 17 Purkinje cells, illustrating the reduced baseline firing during air puff stimulation (Fig. 9C). When we calculated the average complex spike firing for each stimulus condition over the whole population of recorded Purkinje cells, we found that to be remarkably constant. Even 1 Hz air puff stimulation, able to recruit strong complex spike responses, did not result in increased complex spike firing as compared to an epoch without any form of stimulation (Fig. 9D), pointing towards a homeostatic mechanism within the inferior olive that balances out complex spike firing over longer time intervals.

Homeostasis of complex spike firing

To further study the impact of complex spike homeostasis, we averaged the PSTHs of all Purkinje cells with statistically significantly responses to air puff stimulation and compared

these to the firing rate in the absence of stimulation (using pseudo-triggers generated at the same 1 Hz rate). This pair-wise comparison confirmed that the increase in complex spike firing during the sensory-induced responses comes at the expense of inter-trial firing. The same was true for the milder whisker pad stimulation. However, because the responses were weaker, the effect on the inter-trial firing was less than that following strong air puff stimulation. The homeostatic effect was also observed following visual stimulation, although this type of stimulation induced an oscillatory response, making the effect less visible (Fig. 10A-B). Taking the whole population into account, thus also the Purkinje cells without a statistically significant response, there proved to be a correlation between the peak of the stimulus response and the decrease in inter-trial firing ($R = 0.400$; $p = 0.001$ and $R = 0.314$; $p = 0.001$; Pearson correlations for air puff and whisker pad stimulation, respectively; Fig. 10C). Only following visual stimulation, this correlation was less obvious ($R = 0.201$; $p = 0.201$; Pearson correlation after Benjamin-Hochberg correction), possibly due to the oscillatory responses evoked by visual stimulation.

Discussion

Complex spike firing may appear notoriously unpredictable as its spontaneous frequency is low, yet sustained, and its response rate is at best moderate, with large jitters and an ambiguous relation to stimulus strength. This raises the question as to how the inferior olive relays its signals over time. Possibly, coherent complex spike firing by neighbouring Purkinje cells might jointly represent a stimulus, together covering the required signalling for a particular temporal domain (Sasaki *et al.*, 1989; Lang *et al.*, 1999; Sugihara *et al.*, 2007; Ozden *et al.*, 2009; Schultz *et al.*, 2009). Furthermore, the spatial relation between somatotopic patches and parasagittally oriented microzones has not been clarified in terms of complex spike signalling, and it is not understood to what extent this relation also depends on the temporal context in which the signals are generated.

Here, we investigated at the level of individual Purkinje cells whether encoding of somatosensory input from different facial areas in lobule crus 1 occurs in striped microzones or instead follows a more fractured arrangement. Mild touches at localized facial areas revealed a loose version of fractured somatotopy. Purkinje cells with the same receptive field tended to be located in each other's neighbourhood, but the spatial organization was not very strict, as highly responsive Purkinje cells were sometimes observed amidst non-responsive ones. The functionally equivalent, adjacent Purkinje cells showed increased coherence in their complex spike firing, in particular in response to sensory stimulation. Homeostatic mechanisms are engaged, ensuring that over longer periods complex spike firing rates are constant, making the short-lived coherent responses more salient.

The functional role of climbing fibre activity

Clinical manifestations of inferior olivary dysfunction range from ataxia and tremor to autism spectrum disorders (Llinás *et al.*, 1975; Samuel *et al.*, 2004; Bauman & Kemper, 2005; Welsh *et al.*, 2005; Lim & Lim, 2009; De Gruijl *et al.*, 2013). Climbing fibre-evoked complex spikes are also essential for the proper timing, size and direction of movements as well as for the encoding of expected and unexpected deviations from planned movements (Wang *et al.*, 1987; Simpson *et al.*, 1996; Kitazawa *et al.*, 1998; Ito, 2013; Yang & Lisberger, 2014; Herzfeld *et al.*, 2018). In addition, climbing fibre activity is crucial for cerebellar learning by controlling synaptic plasticity at a wide variety of synapses in the molecular layer of the cerebellar cortex (Ito & Kano, 1982; Ito, 2003; Coesmans *et al.*, 2004; Gao *et al.*, 2012).

Despite these many functions, complex spike firing is remarkably stable over longer intervals, suggesting that the impact of complex spikes is strongly context-dependent.

This context is provided by the synaptic inputs to the inferior olive that relay information from excitatory ascending and descending pathways as well as inhibitory projections from the hindbrain (De Zeeuw *et al.*, 1998). Both types converge on each individual spine present on the dendrites of the inferior olivary neurons (De Zeeuw *et al.*, 1989; De Zeeuw *et al.*, 1990). The inhibitory input comes predominantly from the cerebellar nuclei, implying that part of the context is mediated by one of the target regions of the climbing fibres themselves. This feedback is engaged in a closed loop, as individual climbing fibres of each olivary subnucleus project to the Purkinje cells located within a specific parasagittal zone (Sugihara *et al.*, 2001) that converge on the neurons in the cerebellar nuclei that project back to the same olivary subnucleus where the loop started (Groenewegen *et al.*, 1979; Voogd & Glickstein, 1998; Apps *et al.*, 2018). Each module can be further subdivided into microzones within which complex spike coherence is clearly enhanced upon strong stimulation (Ozden *et al.*, 2009; Tsutsumi *et al.*, 2015), a phenomenon that is enhanced by strong electrotonic coupling within olivary glomeruli (Sotelo *et al.*, 1974; Ruigrok *et al.*, 1990; Devor & Yarom, 2002; De Gruijl *et al.*, 2014). Strong stimuli can also increase the coherence of Purkinje cells in adjacent bands (Tsutsumi *et al.*, 2015) while our present data show that weak stimuli can trigger responses of loosely grouped cells not encompassing a full microzone. Thus, although anatomical and functional data support the microzonal organization, the activity patterns are best understood as produced dynamically depending on the behavioural context that is transmitted via cerebellar and extra-cerebellar synaptic input.

Receptive fields of Purkinje cells and population coding

Several existing maps of somatosensory representations of complex spike activity suggest a fractured somatotopy (Miles & Wiesendanger, 1975; Rushmer *et al.*, 1980; Castelfranco *et al.*, 1994). These maps were typically created by establishing, for each recording position, the strongest input region, disregarding information on convergence of multiple inputs. These studies made clear, however, that climbing fibres could have receptive fields of widely different sizes, expanding to structures as large as a whole limb (Thach, 1967). Part of this can be explained by the sagittally fanning climbing projections onto multiple lobules (Sugihara *et al.*, 2001). Here we show with cellular resolution within cerebellar microzones that climbing fibres indeed do convey somatosensory input from different areas, with Purkinje cells having the same receptive fields being located preferably in each other's proximity.

Our data confirm that increasing stimulus strength promotes complex spike responses, but its impact might be lower than predicted by other studies (Eccles *et al.*, 1972; Bosman *et al.*, 2010; Najafi *et al.*, 2014), showing again the relevance of the behavioural and historical context for complex spike firing. More salient than the stimulus strength might be the combination of sensory inputs, in line with the trend of their convergence on single Purkinje cells. Analysing the response rates of Purkinje cell ensembles revealed that the density of responsive cells is crucial for shaping the population response. We propose that the weak spatial clustering of Purkinje cells encoding the same stimulus, being interspersed with Purkinje cells receiving input from other sources, and the tendency of coherent firing of Purkinje cells encoding the same stimulus both contribute to the creation of a heterogeneous map of Purkinje cells, where each area encodes a particular functional set of inputs. Each of the properties of the complex spikes seems rather insignificant in isolation, but in combination may result in specific and robust population encoding.

Non-tactile inputs

Light or sound can act as conditional stimulus to recruit increasingly more climbing fibre activity during learning, highlighting the flexibility of this pathway (Ohmae & Medina, 2015; Ten Brinke *et al.*, 2015). We show here that, also in naïve animals, visual and auditory input can converge on the same Purkinje cells that encode somatosensory input, further strengthening the notion that climbing fibre activity can act as an integrator of contextual input. With visual stimulation the latency was significantly longer than expected. Probably, the presented visual stimulus is not directly relayed from the retina, but a descending input from the visual cortex or other higher brain regions such as the mesodiencephalic junction (De Zeeuw *et al.*, 1998).

Homeostasis of complex spike frequency

The overall firing rate of complex spikes was stable across conditions, with response peaks being compensated by reduced inter-trial firing (see also Warnaar et al. (2018)). The stronger the response peak, the less inter-trial firing, leading to homeostasis of complex spike firing over longer time periods. Intriguingly, the complex spikes during the inter-trial intervals were predominantly fired by a few, dispersed Purkinje cells and the response peak was largely due to increased coherence. It seems therefore that Purkinje cells display a basic complex spike firing rate, which in the absence of functional behaviour is not coherent with adjacent Purkinje cells. In view of the strong impact of complex spikes on synaptic plasticity (Ito &

548 Kano, 1982; Ito, 2003; Coesmans *et al.*, 2004; Gao *et al.*, 2012), this could subserve
549 homeostatic functions. Salient stimuli are largely encoded by coherent firing, making them
550 different from non-stimulus related activity.

551 Several mechanisms may contribute to the homeostatic control of inferior olivary
552 spiking, including the previously mentioned olivo-cerebellar loops. Disrupted Purkinje cell
553 activity can affect climbing fibre activity (Chen *et al.*, 2010) and reduced inferior olivary
554 activity leads to enhanced simple spike activity (Montarolo *et al.*, 1982), which in turn
555 dampens activity in the GABAergic neurons of the cerebellar nuclei that controls the inferior
556 olive (Chaumont *et al.*, 2013; Witter *et al.*, 2013). The interplay between glutamatergic input
557 to the neurons of the inferior olive, intracellular signalling and electrotonic coupling may also
558 lead to homeostatic control of complex spike firing via PKA and ßCaMKII (Mathy *et al.*,
559 2014; Bazzigaluppi *et al.*, 2017). Overall, the inferior olive functions at the cross road of well-
560 defined and rigid anatomical structures and highly dynamic synaptic input, while subject to
561 homeostatic control, the sources of which still are partly to be determined.

562 **References**

563

564 **References**

565 Albus JS. (1971). Theory of cerebellar function. *Math Biosci* **10,** 25-61.

566

567 Andersen P, Eccles JC & Voorhoeve PE. (1964). Postsynaptic inhibition of cerebellar
568 Purkinje cells. *J Neurophysiol* **27,** 1138-1153.

569

570 Apps R & Garwicz M. (2005). Anatomical and physiological foundations of cerebellar
571 information processing. *Nat Rev Neurosci* **6,** 297-311.

572

573 Apps R & Hawkes R. (2009). Cerebellar cortical organization: a one-map hypothesis. *Nat Rev*
574 *Neurosci* **10,** 670-681.

575

576 Apps R, Hawkes R, Aoki S, Bengtsson F, Brown AM, Chen G, Ebner TJ, Isope P, Jorntell H,
577 Lackey EP, Lawrenson C, Lumb B, Schonewille M, Sillitoe RV, Spaeth L, Sugihara I,
578 Valera A, Voogd J, Wylie DR & Ruigrok TJH. (2018). Cerebellar modules and their
579 role as operational cerebellar processing units. *Cerebellum*.

580

581 Arabzadeh E, Panzeri S & Diamond ME. (2004). Whisker vibration information carried by rat
582 barrel cortex neurons. *J Neurosci* **24,** 6011-6020.

583

584 Axelrad H & Crepel F. (1977). Représentation sélective des vibrisses mystaciales au niveau
585 des cellules de Purkinje du cervelet par la voie des fibres grimpantes chez le rat. *C R*
586 *Acad Sci Hebd Seances Acad Sci D* **284,** 1321-1324.

587

588 Bauman ML & Kemper TL. (2005). Neuroanatomic observations of the brain in autism: a
589 review and future directions. *Int J Dev Neurosci* **23,** 183-187.

590

591 Bazzigaluppi P, Isenia SC, Haasdijk ED, Elgersma Y, De Zeeuw CI, van der Giessen RS & de
592 Jeu MTG. (2017). Modulation of murine olivary connexin 36 gap Junctions by PKA
593 and CaMKII. *Front Cell Neurosci* **11,** 397.

594

595 Bloedel JR & Ebner TJ. (1984). Rhythmic discharge of climbing fibre afferents in response to
596 natural peripheral stimuli in the cat. *J Physiol* **352,** 129-146.

597

598 Bosman LWJ, Houweling AR, Owens CB, Tanke N, Shevchouk OT, Rahmati N, Teunissen
599 WHT, Ju C, Gong W, Koekkoek SKE & De Zeeuw CI. (2011). Anatomical pathways
600 involved in generating and sensing rhythmic whisker movements. *Front Integr*
601 *Neurosci* **5,** 53.

602

603 Bosman LWJ, Koekkoek SKE, Shapiro J, Rijken BFM, Zandstra F, van der Ende B, Owens
604 CB, Potters JW, de Gruijl JR, Ruigrok TJH & De Zeeuw CI. (2010). Encoding of
605 whisker input by cerebellar Purkinje cells. *J Physiol* **588,** 3757-3783.

606
607 Brown IE & Bower JM. (2002). The influence of somatosensory cortex on climbing fiber
608 responses in the lateral hemispheres of the rat cerebellum after peripheral tactile
609 stimulation. *J Neurosci* **22,** 6819-6829.

610
611 Castelfranco AM, Robertson LT & McCollum G. (1994). Detail, proportion, and foci among
612 face receptive fields of climbing fiber responses in the cat cerebellum. *Somatosens*
613 *Mot Res* **11,** 27-46.

614
615 Cerminara NL, Lang EJ, Sillitoe RV & Apps R. (2015). Redefining the cerebellar cortex as an
616 assembly of non-uniform Purkinje cell microcircuits. *Nat Rev Neurosci* **16,** 79-93.

617
618 Chaplan SR, Bach FW, Pogrel JW, Chung JM & Yaksh TL. (1994). Quantitative assessment
619 of tactile allodynia in the rat paw. *J Neurosci Methods* **53,** 55-63.

620
621 Chaumont J, Guyon N, Valera AM, Dugué GP, Popa D, Marcaggi P, Gautheron V, Reibel-
622 Foisset S, Dieudonné S, Stephan A, Barrot M, Cassel JC, Dupont JL, Doussau F,
623 Poulain B, Selimi F, Léna C & Isope P. (2013). Clusters of cerebellar Purkinje cells
624 control their afferent climbing fiber discharge. *Proc Natl Acad Sci U S A* **110,** 16223-
625 16228.

626
627 Chen X, Kovalchuk Y, Adelsberger H, Henning HA, Sausbier M, Wietzorrek G, Ruth P,
628 Yarom Y & Konnerth A. (2010). Disruption of the olivo-cerebellar circuit by Purkinje
629 neuron-specific ablation of BK channels. *Proc Natl Acad Sci U S A* **107,** 12323-12328.

630
631 Coesmans M, Weber JT, De Zeeuw CI & Hansel C. (2004). Bidirectional parallel fiber
632 plasticity in the cerebellum under climbing fiber control. *Neuron* **44,** 691-700.

633
634 De Gruijl JR, Bosman LWJ, De Zeeuw CI & De Jeu MTG. (2013). Inferior olive: All ins and
635 outs. In *Handbook of the Cerebellum and Cerebellar Disorders*, ed. Manto M,
636 Schmahmann JD, Rossi F, Gruol DL & Koibuchi N, pp. 1013-1058. Springer
637 Netherlands, Dordrecht.

638
639 De Gruijl JR, Hoogland TM & De Zeeuw CI. (2014). Behavioral correlates of complex spike
640 synchrony in cerebellar microzones. *J Neurosci* **34,** 8937-8944.

641
642 De Zeeuw CI, Hoebeek FE, Bosman LWJ, Schonewille M, Witter L & Koekkoek SK. (2011).
643 Spatiotemporal firing patterns in the cerebellum. *Nat Rev Neurosci* **12,** 327-344.

644

De Zeeuw CI, Holstege JC, Ruigrok TJ & Voogd J. (1989). Ultrastructural study of the GABAergic, cerebellar, and mesodiencephalic innervation of the cat medial accessory olive: anterograde tracing combined with immunocytochemistry. *J Comp Neurol* **284,** 12-35.

De Zeeuw CI, Holstege JC, Ruigrok TJH & Voogd J. (1990). Mesodiencephalic and cerebellar terminals terminate upon the same dendritic spines in the glomeruli of the cat and rat inferior olive: an ultrastructural study using a combination of [3H]leucine and wheat germ agglutinin coupled horseradish peroxidase anterograde tracing. *Neuroscience* **34,** 645-655.

De Zeeuw CI, Simpson JI, Hoogenraad CC, Galjart N, Koekkoek SKE & Ruigrok TJH. (1998). Microcircuitry and function of the inferior olive. *Trends Neurosci* **21,** 391-400.

De Zeeuw CI & Ten Brinke MM. (2015). Motor learning and the cerebellum. *Cold Spring Harb Perspect Biol* **7,** a021683.

Devor A & Yarom Y. (2002). Electrotonic coupling in the inferior olivary nucleus revealed by simultaneous double patch recordings. *J Neurophysiol* **87,** 3048-3058.

Eccles JC, Sabah NH, Schmidt RF & Táboríková H. (1972). Cutaneous mechanoreceptors influencing impulse discharges in cerebellar cortex. III. In Purkyně cells by climbing fiber input. *Exp Brain Res* **15,** 484-497.

Ekerot CF, Garwicz M & Schouenborg J. (1991). Topography and nociceptive receptive fields of climbing fibres projecting to the cerebellar anterior lobe in the cat. *J Physiol* **441,** 257-274.

Gao W, Chen G, Reinert KC & Ebner TJ. (2006). Cerebellar cortical molecular layer inhibition is organized in parasagittal zones. *J Neurosci* **26,** 8377-8387.

Gao Z, Van Beugen BJ & De Zeeuw CI. (2012). Distributed synergistic plasticity and cerebellar learning. *Nat Rev Neurosci* **13,** 619-635.

Gibson AR, Horn KM & Pong M. (2004). Activation of climbing fibers. *Cerebellum* **3,** 212-221.

Groenewegen HJ, Voogd J & Freedman SL. (1979). The parasagittal zonation within the olivocerebellar projection. II. Climbing fiber distribution in the intermediate and hemispheric parts of cat cerebellum. *J Comp Neurol* **183,** 551-601.

686 Harvey RJ & Napper RMA. (1991). Quantitative studies on the mammalian cerebellum. *Prog*
687 *Neurobiol* **36,** 437-463.

688
689 Herzfeld DJ, Kojima Y, Soetedjo R & Shadmehr R. (2018). Encoding of error and learning to
690 correct that error by the Purkinje cells of the cerebellum. *Nat Neurosci* **21,** 736-743.

691
692 Hoogland TM, De Gruijl JR, Witter L, Canto CB & De Zeeuw CI. (2015). Role of
693 synchronous activation of cerebellar Purkinje cell ensembles in multi-joint movement
694 control. *Curr Biol* **25,** 1157-1165.

695
696 Ito M. (2003). Long-term depression. *Annu Rev Neurosci* **12,** 85-102.

697
698 Ito M. (2013). Error detection and representation in the olivo-cerebellar system. *Front Neural*
699 *Circuits* **7,** 1.

700
701 Ito M & Kano M. (1982). Long-lasting depression of parallel fiber-Purkinje cell transmission
702 induced by conjunctive stimulation of parallel fibers and climbing fibers in the
703 cerebellar cortex. *Neurosci Lett* **33,** 253-258.

704
705 Junker M, Endres D, Sun ZP, Dicke PW, Giese M & Thier P. (2018). Learning from the past:
706 A reverberation of past errors in the cerebellar climbing fiber signal. *PLoS Biol* **16,**
707 e2004344.

708
709 Khosrovani S, Van Der Giessen RS, De Zeeuw CI & De Jeu MTG. (2007). *In vivo* mouse
710 inferior olive neurons exhibit heterogeneous subthreshold oscillations and spiking
711 patterns. *Proc Natl Acad Sci U S A* **104,** 15911-15916.

712
713 Kitazawa S, Kimura T & Yin PB. (1998). Cerebellar complex spikes encode both destinations
714 and errors in arm movements. *Nature* **392,** 494-497.

715
716 Kubo R, Aiba A & Hashimoto K. (2018). The anatomical pathway from the mesodiencephalic
717 junction to the inferior olive relays perioral sensory signals to the cerebellum in the
718 mouse. *J Physiol*.

719
720 Lang EJ, Sugihara I, Welsh JP & Llinás R. (1999). Patterns of spontaneous purkinje cell
721 complex spike activity in the awake rat. *J Neurosci* **19,** 2728-2739.

722
723 Lim CCT & Lim SA. (2009). Pendular nystagmus and palatomyoclonus from hypertrophic
724 olivary degeneration. *New Engl J Med* **360,** e12.

725
726 Llinás R, Walton K, Hillman DE & Sotelo C. (1975). Inferior olive: its role in motor learing.
727 *Science* **190,** 1230-1231.

Mathy A, Clark BA & Häusser M. (2014). Synaptically induced long-term modulation of electrical coupling in the inferior olive. *Neuron* **81,** 1290-1296.

Miles TS & Wiesendanger M. (1975). Organization of climbing fibre projections to the cerebellar cortex from trigeminal cutaneous afferents and from the SI face area of the cerebral cortex in the cat. *J Physiol* **245,** 409-424.

Montarolo PG, Palestini M & Strata P. (1982). The inhibitory effect of the olivocerebellar input on the cerebellar Purkinje cells in the rat. *J Physiol* **332,** 187-202.

Mukamel EA, Nimmerjahn A & Schnitzer MJ. (2009). Automated analysis of cellular signals from large-scale calcium imaging data. *Neuron* **63,** 747-760.

Najafi F, Giovannucci A, Wang SSH & Medina JF. (2014). Coding of stimulus strength via analog calcium signals in Purkinje cell dendrites of awake mice. *eLIFE* **3,** e03663.

Najafi F & Medina JF. (2013). Beyond "all-or-nothing" climbing fibers: graded representation of teaching signals in Purkinje cells. *Front Neural Circuits* **7,** 115.

Ohmae S & Medina JF. (2015). Climbing fibers encode a temporal-difference prediction error during cerebellar learning in mice. *Nat Neurosci* **18,** 1798-1803.

Oscarsson O. (1969). Termination and functional organization of the dorsal spino-olivocerebellar path. *J Physiol* **200,** 129-149.

Ozden I, Dombeck DA, Hoogland TM, Tank DW & Wang SS. (2012). Widespread state-dependent shifts in cerebellar activity in locomoting mice. *PLoS One* **7,** e42650.

Ozden I, Lee HM, Sullivan MR & Wang SSH. (2008). Identification and clustering of event patterns from in vivo multiphoton optical recordings of neuronal ensembles. *J Neurophysiol* **100,** 495-503.

Ozden I, Sullivan MR, Lee HM & Wang SSH. (2009). Reliable coding emerges from coactivation of climbing fibers in microbands of cerebellar Purkinje neurons. *J Neurosci* **29,** 10463-10473.

Person AL & Raman IM. (2011). Purkinje neuron synchrony elicits time-locked spiking in the cerebellar nuclei. *Nature* **481,** 502-505.

Romano V, De Propris L, Bosman LWJ, Warnaar P, Ten Brinke MM, Lindeman S, Ju C, Velauthapillai A, Spanke JK, Middendorp Guerra E, Hoogland TM, Negrello M,

D'Angelo E & De Zeeuw CI. (2018). Potentiation of cerebellar Purkinje cells facilitates whisker reflex adaptation through increased simple spike activity. *bioRxiv***,** 335489.

Ruigrok TJH. (2011). Ins and outs of cerebellar modules. *Cerebellum* **10,** 464-474.

Ruigrok TJH, de Zeeuw CI, van der Burg J & Voogd J. (1990). Intracellular labeling of neurons in the medial accessory olive of the cat: I. Physiology and light microscopy. *J Comp Neurol* **300,** 462-477.

Rushmer DS, Woollacott MH, Robertson LT & Laxer KD. (1980). Somatotopic organization of climbing fiber projections from low threshold cutaneous afferents to pars intermedia of cerebellar cortex in the cat. *Brain Res* **181,** 17-30.

Samuel M, Torun N, Tuite PJ, Sharpe JA & Lang AE. (2004). Progressive ataxia and palatal tremor (PAPT): clinical and MRI assessment with review of palatal tremors. *Brain* **127,** 1252-1268.

Sasaki K, Bower JM & Llinás R. (1989). Multiple Purkinje cell recording in rodent cerebellar cortex. *Eur J Neurosci* **1,** 572-586.

Schultz SR, Kitamura K, Post-Uiterweer A, Krupic J & Häusser M. (2009). Spatial pattern coding of sensory information by climbing fiber-evoked calcium signals in networks of neighboring cerebellar Purkinje cells. *J Neurosci* **29,** 8005-8015.

Shambes GM, Gibson JM & Welker W. (1978). Fractured somatotopy in granule cell tactile areas of rat cerebellar hemispheres revealed by micromapping. *Brain Behav Evol* **15,** 94-140.

Simpson JI, Wylie DR & De Zeeuw CI. (1996). On climbing fiber signals and their consequence(s). *Behav Brain Sci* **19,** 384-398.

Sotelo C, Llinás R & Baker R. (1974). Structural study of inferior olivary nucleus of the cat: morphological correlates of electrotonic coupling. *J Neurophysiol* **37,** 541-559.

Stosiek C, Garaschuk O, Holthoff K & Konnerth A. (2003). *In vivo* two-photon calcium imaging of neuronal networks. *Proc Natl Acad Sci U S A* **100,** 7319-7324.

Streng ML, Popa LS & Ebner TJ. (2017). Climbing fibers control Purkinje cell representations of behavior. *J Neurosci* **37,** 1997-2009.

Sugihara I, Fujita H, Na J, Quy PN, Li BY & Ikeda D. (2009). Projection of reconstructed single Purkinje cell axons in relation to the cortical and nuclear aldolase C compartments of the rat cerebellum. *J Comp Neurol* **512,** 282-304.

Sugihara I, Marshall SP & Lang EJ. (2007). Relationship of complex spike synchrony bands and climbing fiber projection determined by reference to aldolase C compartments in crus IIa of the rat cerebellar cortex. *J Comp Neurol* **501,** 13-29.

Sugihara I, Wu H & Shinoda Y. (1999). Morphology of single olivocerebellar axons labeled with biotinylated dextran amine in the rat. *J Comp Neurol* **414,** 131-148.

Sugihara I, Wu HS & Shinoda Y. (2001). The entire trajectories of single olivocerebellar axons in the cerebellar cortex and their contribution to cerebellar compartmentalization. *J Neurosci* **21,** 7715-7723.

Sullivan MR, Nimmerjahn A, Sarkisov DV, Helmchen F & Wang SSH. (2005). In vivo calcium imaging of circuit activity in cerebellar cortex. *J Neurophysiol* **94,** 1636-1644.

Suvrathan A, Payne HL & Raymond JL. (2016). Timing rules for synaptic plasticity matched to behavioral function. *Neuron* **92,** 959-967.

Szentágothai J. (1965). The use of degeneration methods in the investigation of short neuronal connexions. *Prog Brain Res* **14,** 1-32.

Tada M, Takeuchi A, Hashizume M, Kitamura K & Kano M. (2014). A highly sensitive fluorescent indicator dye for calcium imaging of neural activity *in vitro* and *in vivo*. *Eur J Neurosci* **39,** 1720-1728.

Ten Brinke MM, Boele HJ, Spanke JK, Potters JW, Kornysheva K, Wulff P, IJpelaar ACHG, Koekkoek SKE & De Zeeuw CI. (2015). Evolving models of Pavlovian conditioning: cerebellar cortical dynamics in awake behaving mice. *Cell Rep* **13,** 1977-1988.

Thach WT, Jr. (1967). Somatosensory receptive fields of single units in cat cerebellar cortex. *J Neurophysiol* **30,** 675-696.

Tsutsumi S, Yamazaki M, Miyazaki T, Watanabe M, Sakimura K, Kano M & Kitamura K. (2015). Structure-function relationships between aldolase C/zebrin II expression and complex spike synchrony in the cerebellum. *J Neurosci* **35,** 843-852.

Voogd J & Glickstein M. (1998). The anatomy of the cerebellum. *Trends Neurosci* **21,** 370-375.

Wang JJ, Kim JH & Ebner TJ. (1987). Climbing fiber afferent modulation during a visually guided, multi-joint arm movement in the monkey. *Brain Res* **410,** 323-329.

Warnaar P, Negrello M, Romano V, Owens CB, Lindeman S, Iavarona E, Spanke JK, Bosman LWJ & De Zeeuw CI. (2018). Aperiodic rhythms of the inferior olive. *bioRxiv***,** 408112.

Welsh JP, Ahn ES & Placantonakis DG. (2005). Is autism due to brain desynchronization? *Int J Dev Neurosci* **23,** 253-263.

Welsh JP, Lang EJ, Suglhara I & Llinas R. (1995). Dynamic organization of motor control within the olivocerebellar system. *Nature* **374,** 453-457.

Witter L, Canto CB, Hoogland TM, de Gruijl JR & De Zeeuw CI. (2013). Strength and timing of motor responses mediated by rebound firing in the cerebellar nuclei after Purkinje cell activation. *Front Neural Circuits* **7,** 133.

Xiao J, Cerminara NL, Kotsurovskyy Y, Aoki H, Burroughs A, Wise AK, Luo Y, Marshall SP, Sugihara I, Apps R & Lang EJ. (2014). Systematic regional variations in Purkinje cell spiking patterns. *PLoS One* **9,** e105633.

Yang Y & Lisberger SG. (2014). Purkinje-cell plasticity and cerebellar motor learning are graded by complex-spike duration. *Nature* **510,** 529-532.

Yatim N, Billig I, Compoint C, Buisseret P & Buisseret-Delmas C. (1996). Trigeminocerebellar and trigemino-olivary projections in rats. *Neurosci Res* **25,** 267-283.

Zhou H, Lin Z, Voges K, Ju C, Gao Z, Bosman LWJ, Ruigrok TJH, Hoebeek FE, De Zeeuw CI & Schonewille M. (2014). Cerebellar modules operate at different frequencies. *eLIFE* **3,** e02536.

Additional information

Competing interests

The authors declare that there are no competing interests.

Author contributions

All experiments were performed at the Department of Neuroscience of the Erasmus MC, Rotterdam, The Netherlands. The experiments were designed by C.J., L.W.J.B., T.M.H., P.M., M.N. and C.I.D.Z., performed by C.J. and P.M. and analysed by all authors. The manuscript was written by C.J., L.W.J.B., T.M.H., M.N. and C.I.D.Z. with contributions from all authors. All authors have approved the final version of the manuscript and ensure the accuracy and integrity of the data presented. All persons with a significant contribution to this study are listed as authors.

Funding

Financial support was provided by the Netherlands Organization for Scientific Research (NWO-ALW; C.I.D.Z.), the Dutch Organization for Medical Sciences (ZonMW; C.I.D.Z.), Life Sciences (C.I.D.Z.), ERC-adv and ERC-POC (C.I.D.Z.) and the China Scholarship Council (No. 2010623033; C.J.). The funders had no role in study design, data collection and analysis, decision to publish, or preparation of the manuscript.

Acknowledgements

The authors wish to thank A.C.H.G. IJpelaar for technical assistance and Dr. M. Schonewille for help with recording ocular movements during stimulation.

912 **Tables**

913 **Table 1**

Stimulation	Responsive cells		Response parameters		Prevalence (*p*) χ^2 = 25.758; df = 5; *p* = 0.001				
	No.	**%**	**Peak (Hz)**	**Latency (ms)**	**UL**	**LL**	**Ch**	**SO**	**LED**
Whisker pad	111 (282)	39	2.12 ± 0.82	84±42	**0.010**	0.661	**0.003**	**0.000**	0.828
Upper lip	71 (249)	29	1.89 ± 0.67	84±84		**0.031**	0.597	0.157	0.064
Lower lip	99 (264)	38	2.23 ± 0.97	84±42			**0.010**	**0.001**	1.000
Cheek	53 (203)	26	2.30 ± 1.67	84±42				0.415	**0.028**
Sound only	44 (197)	22	1.74 ± 0.65	84±84					**0.003**
LED	49 (129)	34	2.13 ± 1.18	126±0					

914

915 **Table 1 – Purkinje cell responses to sensory stimulation in awake mice**

916 Purkinje cells respond with complex firing to sensory stimulation (Fig. 3). For each type of
917 stimulation, the number and percentage of statistically significantly responsive cells (peak
918 response > average + 3 s.d. of baseline firing) is indicated (in brackets: total number of cells
919 tested). The response peak and response latency are indicated as medians ± inter-quartile
920 ranges. The relative prevalence of responses was not equal for all stimulus types, as
921 confirmed by a 6x2 χ^2 test. Differences in relative prevalence were tested using pair-wise
922 Fisher's exact tests (as the χ^2 test was significant, no further correction for multiple
923 comparisons was applied). Bold values indicate significantly different prevalences. UL =
924 upper lip; LL = lower lip; CH = cheek; SO = sound only.

925 **Table 2**

Stimulation	Pearson correlation (R)					Significance of Pearson correlation (*p*)				
	UL	**LL**	**Ch**	**SO**	**LED**	**UL**	**LL**	**Ch**	**SO**	**LED**
Whisker pad	0.272	0.253	0.166	0.257	0.358	**<0.001**	**<0.001**	**0.018**	**0.001**	**<0.001**
Upper lip		0.192	0.189	0.130	0.129		**0.002**	**0.001**	0.126	0.179
Lower lip			0.387	0.513	0.339			**<0.001**	**<0.001**	**<0.001**
Cheek				0.485	0.362				**<0.001**	**<0.001**
Sound only					0.523					**<0.001**

926

927 **Table 2 – Correlations between response probabilities**

928 For each Purkinje cell, we made pair-wise correlations of the Z scores of the amplitudes of the
929 responses to different stimuli. The Pearson correlation coefficient (R) and the accompanying *p*
930 value are indicated in this Table. The *p* values indicated in bold reflect significant values
931 (after Benajmini-Hochberg correction for multiple comparisons). These data are graphically
932 represented in Fig. 4A. WP = whisker pad; UL = upper lip; LL = lower lip; Ch = cheek; SO =
933 sound only.

934

935 **Table 3**

Stimulation	Rate of occurrence (*Z*)					Chance of occurrence (*p*)				
	UL	**LL**	**Ch**	**SO**	**LED**	**UL**	**LL**	**Ch**	**SO**	**LED**
Whisker pad	1.21	1.25	0.85	1.34	**2.75**	0.225	0.213	0.394	0.181	**0.006**
Upper lip		1.23	**2.00**	1.34	1.94		0.220	**0.045**	0.181	0.052
Lower lip			**2.39**	**2.70**	**2.62**			**0.017**	**0.007**	**0.009**
Cheek				**3.31**	**3.10**				**0.001**	**0.002**
Sound only					**2.28**					**0.022**

936

937 **Table 3 – Convergence of different sensory streams on individual Purkinje cells**

938 For each type of stimulus, we compared the observed rate of convergence on individual
939 Purkinje cells to chance level, using a bootstrap method based on the relative prevalence of
940 each stimulus (cf. Fig. 4). Indicated are the *Z* and the *p* values. All combinations occurred
941 more often than expected ($Z > 0$). Bold values indicate statistical significance. WP = whisker
942 pad; UL = upper lip; LL = lower lip; Ch = cheek; SO = sound only.

943 **Table 4**

Stimulation	Rate of occurrence (*Z*)	Chance of occurrence (*p*)
WP + UL + LL	1.89	0.059
WP + LL + Ch	1.32	0.186
UL + LL + Ch	3.22	**0.001**
WP + UL + LL + Ch	3.07	**0.002**

944

945 **Table 4 – Convergence of different sensory streams on individual Purkinje cells**

946 For each type of stimulus, we compared the observed rate of convergence on individual
947 Purkinje cells to chance level, using a bootstrap method based on the relative prevalence of
948 each stimulus (cf. Fig. 4). Indicated are the *Z* and the *p* values. All combinations occurred
949 more often than expected ($Z > 0$). Bold values indicate statistical significance. WP = whisker
950 pad; UL = upper lip; LL = lower lip; Ch = cheek.

951

952 **Table 5**

Whisker	Responsive cells		Rate of occurrence (*Z*)				Prevalence (*p*)			
	No.	**%**	**C1**	**C2**	**C3**	**D2**	**C1**	**C2**	**C3**	**D2**
B2	15 (148)	10	0.630	0.227	**5.130**	**2.052**	0.264	0.410	**<0.001**	0.020
C1	4 (148)	3		0.803	0.782	0.630		0.211	0.217	0.264
C2	17 (148)	11			0.222	0.208			0.412	0.418
C3	23 (148)	16				**3.100**				**0.001**
D2	15 (148)	10								

953

954 **Table 5 – Purkinje cell responses to single-whisker stimulation in anaesthetized mice**

955 Purkinje cells respond with complex firing to single-whisker stimulation (cf. Figure 4). For
956 each whisker, the number and percentage of responsive cells is indicated (in brackets: total
957 number of cells tested). For each whisker, we compared the observed rate of convergence on
958 individual Purkinje cells to chance level, using a bootstrap methods based on the relative
959 prevalence of each stimulus. Indicated are the *Z* and the *p* values. All combinations occurred
960 more often than expected ($Z > 0$). Bold values indicate statistical significance after Benjamini-
961 Hochberg correction for multiple comparisons.

962

963 **Figure legends**

964

965 **Figure 1 – Sensory pathways carrying facial input to the cerebellar cortex**

966 **(A)** Scheme of the main routes conveying facial tactile input via the climbing fibre pathway to
967 cerebellar Purkinje cells (PC). Climbing fibres, which cause complex spike firing in Purkinje
968 cells, exclusively originate from the inferior olive. The inferior olive, in turn, is directly
969 innervated by neurons from the trigeminal nuclei as well as indirectly via thalamo-cortical
970 pathways that project to the inferior olive mainly via the nuclei of the mesodiencephalic
971 junction (MDJ). The MDJ itself also receives direct input from the trigeminal nuclei. See the
972 main text for references. **(B)** *In vivo* two-photon Ca^{2+} imaging was performed to characterize
973 Purkinje cell complex spike responses to sensory stimulation in the medial part of crus 1.
974 Purkinje cells were detected using independent component analysis and the position of a
975 Purkinje cell dendrite (yellow area on the right) within a field of view is shown in the inset. At
976 the end of each recording session, the brain was removed and the location of the dye injection
977 in medial crus 1 was confirmed through *ex vivo* epifluorescent imaging (black circle). The
978 white rectangle indicates the approximate recording location. **(C)** Complex spikes that were
979 triggered by climbing fibre activity were retrieved from fluorescent traces of individual
980 Purkinje cells. A representative trace obtained from the Purkinje cell dendrite illustrated in **B**
981 is shown together with the detected complex spikes (grey lines). The light blue episode is
982 enlarged in **D**. Complex spikes were detected by the combination of a threshold and a
983 template matching algorithm. Only events with a sharp rising phase were accepted as complex
984 spikes. In the 60 s interval shown in **C**, there was one event with a slower rise time (see arrow
985 in **D**), as indicated at a larger time scale in **E**. The events in **E** are scaled to peak.

986

987 **Figure 2 - Whisker stimulation evokes complex spike responses in cerebellar crus 1**

988 **(A)** Complex spikes elicit large increases in the Ca^{2+} concentration within Purkinje cell
989 dendrites that can be resolved using *in vivo* two-photon microscopy in combination with a
990 fluorescent Ca^{2+} indicator. An example of a field of view with 19 identified Purkinje cell
991 dendrites located in the medial part of crus 1 is shown with each individual dendrite denoted
992 by a number and a unique colour. This recording was made in an awake mouse. **(B)** The
993 fluorescent traces of each of these dendrites show distinct Ca^{2+} transient events, which are to a
994 large extent associated with air puff stimulation of the facial whiskers (times of stimulation
995 indicated by the vertical lines). The boxed area is enlarged in Fig. S1. **(C)** Summed
996 fluorescence trace composed of all 19 individual traces emphasizing the participation of many

Purkinje cells to the stimulus-triggered responses. **(D)** After complex spike extraction, a clear relation between stimulus and activity was observed as illustrated by summing, for each frame, the number of complex spikes observed over all dendrites. The vertical scale bar corresponds to the simultaneous activity of 5 Purkinje cells. **(E)** Peri-stimulus time histogram of a Purkinje cell dendrite (marked as number 7 in **A** and **B**) in response to air puff stimulation to the ipsilateral whiskers (154 trials). The bin size (40 ms) corresponds to the acquisition frame rate (25 Hz). **(F)** Normalized stacked line graph of the Purkinje cells in this field of view showing that every cell contributed to the overall response. The Purkinje cells are ranked by their maximal response and the data are normalized so that the top line reflects the average frequency per bin. Cell no. 7 (dashed line) had a relatively poor signal-to-noise ratio during later parts of the recording (see Fig. S1), but it had nevertheless a complex spike response profile that was indistinguishable from the other cells. The colours match those in the panels **A**-**B**. Inset: In total, 102 out of 117 cells analysed (87%) were responsive to whisker air puff stimulation (peak response exceeded average + 3 s.d. of pre-stimulus interval). **(G)** Fluorescent traces of the trials with (red) and without (black) complex spikes fired during the first 200 ms after air puff onset. In the absence of complex spike firing, only a very small increase in fluorescence was observed, indicating that the majority of change in fluorescence was associated with complex spike firing. Note the longer time scale than in **E** and **F**. The lines indicate the medians and the shaded areas the inter-quartile ranges of the 19 Purkinje cells in this field of view.

Figure 3 – Purkinje cells in crus 1 respond to various types of sensory stimulation

(A) Tactile stimuli were presented to four facial regions in awake mice: the whisker pad (WP), the upper lip (UL), the lower lip (LL) and the cheek (Ch). Each stimulus was delivered with a piezo-actuator that made a muted, yet audible sound which was also delivered without touch ("sound only (SO)"). A blue light flash generated by an LED was used as visual stimulus. These experiments were performed in awake mice. **(B)** To avoid interference of adjacent areas, we applied gentle touches (0.686 mN). The complex spike response ratio was much reduced relative to the strong air puff stimulation to all ipsilateral whiskers illustrated in Fig. 2. A histogram of the peak responses (expressed as Z value) of all responses to either of the four tactile stimuli demonstrates that the response strength is a continuum, showing the lack of a clear separation between "responsive" and "non-responsive" Purkinje cells (998 stimulus conditions in 282 Purkinje cells). We considered Purkinje cells that showed a peak response above Z = 3 as "significantly responsive" (represented with black bars), but we

provide most of the analyses also for the population as a whole (e.g., Fig. S2). **(C)** The peri-stimulus time histograms (PSTHs) of a representative Purkinje cell. The shades of grey indicate 1, 2 and 3 s.d. around the average. Each stimulus was repeated 154 times at 1 Hz. **(D)** For every stimulus condition, we averaged the PSTHs for all Purkinje cells that were significantly responsive to that particular stimulus (coloured lines; median (inter-quartile range)). These were contrasted to the averaged PSTH of the other Purkinje cells (black lines). The pie charts represent the fraction of Purkinje cells significantly responsive to a particular stimulus. See also Table 1. **(E)** The peak responses of the significantly responding Purkinje cells were the lowest for sound only and for upper lip stimulation. * $p < 0.05$; ** $p < 0.01$ (post-hoc tests after Kruskal-Wallis test) **(F)** As expected for complex spike responses to weak stimulation, the latencies were relatively long and variable, but consistent across types of stimulation. Only visual stimulation (LED) had a remarkably longer latency time. *** $p < 0.001$ (post-hoc tests after Kruskal-Wallis test for LED vs. whisker pad, upper lip, lower lip and cheek and $p < 0.05$ compared to sound only)

Figure 4 – Convergence of sensory input on Purkinje cells

(A) In order to test whether sensory inputs converge on individual Purkinje cells in awake mice, we made pair-wise comparisons of the response amplitudes to two different stimuli per Purkinje cell (scatter plots). For all possible combinations, we found a positive slope of the correlation analysis. For the majority of combinations, the correlation between response strengths was highly significant: * $p < 0.05$, ** $p < 0.01$ and *** $p < 0.001$ (Pearson correlation with Benjamini-Hochberg correction for multiple comparisons). Only upper lip vs. sound only and upper lip vs. visual stimulation were not significantly correlated. For this analysis, we included all Purkinje cells, whether they had a statistically significant response or not. The red dotted lines indicate a Z-score of 3, which we set as the threshold for significance (cf. Fig. 3B). They grey arrows indicate the fraction of observations above and below the unity line (grey dotted line). The relative strengths of every stimulus combination were compared in a pairwise fashion (Wilcoxon tests with Benjamini-Hochberg correction for multiple comparisons): & $p < 0.05$; && $p < 0.01$; &&& $p < 0.001$. **(B)** We performed a similar analysis focusing only on statistically significant responses (Venn diagrams). Again, all combinations had a positive Z score (as evaluated by a bootstrap method; see Methods), indicating more than expected convergence. The diameter of each circle indicates the fraction of Purkinje cells showing a significant response to that particular, colour coded stimulus. The size of the bar represents the Z score of the overlapping fraction. **(C)** The same for the

combinations of three tactile stimuli. Overall, sensory streams tended to converge, rather than diverge, on Purkinje cells. # $p < 0.10$; * $p < 0.05$, ** $p < 0.01$ and *** $p < 0.001$ (Z test with Benjamini-Hochberg correction).

Figure 5 – Stimulus strength has only a minor impact on complex spike responsiveness

(A) Movements of all large facial whiskers were performed using a piezo-actuator at three different speeds (weak: 1 mm displacement in 62 ms; moderate: 2 mm displacement in 31 ms; strong: 4 mm displacement in 16 ms). The stimulus sequence was randomly permuted. The recordings were made in awake mice. **(B)** Field of view with 24 identified and colour-coded Purkinje cells (left) and their corresponding fluorescent traces (right). Stimuli were presented every 2 s and in between trials the laser illumination was briefly blocked to avoid photobleaching. Note that the periods without laser illumination are not drawn to scale. The vertical shaded areas indicate stimulus duration (which was inverse with the stimulus strength). **(C)** Summed fluorescence trace composed of all 24 individual traces showing that not all trials evoked ensemble-wide responses. Some spontaneous, inter-trial activity was also observed. **(D)** The median number of complex spikes per frame (of 40 ms) per trial (shaded areas: inter-quartile range) for the three stimulus strengths show little difference for the weak and moderate stimulation. The time course and amplitude (1-4 mm) of the three stimuli is schematized at the bottom of the graph. Strong stimulation elicited about 30% more complex spikes, as evident from the peak responses for each stimulus intensity. **(E)** Plotting for each of Purkinje cell the average peak response for each stimulus condition results in many overlapping lines. Only a few cells stand out in that they show a strong response that consistently increases with stimulus strength (red lines on top). The Purkinje cells that showed increased responsiveness to stronger stimuli are depicted in red and the others in blue (see also Fig. S4A). **(F)** The same data summarized with box plots for all significantly responsive cells. Data are from 209 significantly responsive Purkinje cells (out of 340 Purkinje cells that were measured in this way). *** $p < 0.001$ (Friedman's test).

Figure 6 - Purkinje cells encoding the same stimulus have a tendency to be spatially grouped

Schematic drawing of a field of view with 26 Purkinje cells organized in the medio-lateral direction of crus 1 in an awake mouse. The colour of each Purkinje cell corresponds to the maximal response to whisker pad **(A)** or upper lip **(B)** stimulation. Purkinje cells with a filled soma had a peak response with a Z score > 3 and were considered to be statistically

significant, in contrast to those with an open soma. Responsive and non-responsive cells are generally intermingled, but a group of "strong responders" can be observed for whisker pad stimulation (red rectangle). **(C)** The anecdotal data in **A** suggest the presence of clusters of Purkinje cells encoding specific stimuli. For this to be the case, one would expect that neighbouring Purkinje cells have roughly similar response strengths. We found that this assumption does not hold as the differences in response strengths of neighbours could not be discriminated from randomly selected cells in the same recording if all Purkinje cells are considered (compared with bootstrap analysis based upon randomly chosen cell pairs within each field of view: all $p > 0.8$; Z test). Data are represented in violin plots, with the grey lines indicating the 10^{th}, 25^{th}, 50^{th}, 75^{th} and 90^{th} percentiles. **(D)** When considering only the Purkinje cells with statistically significant responses, spatial grouping does occur. For each stimulus type, the black portion of the left bar indicates the fraction of Purkinje cells showing a significant response to that stimulus. The filled portion of the right bar indicates the fraction of the neighbours (always on the medial side) of these significantly responsive Purkinje cells that were also significantly responsive. As can be seen, this fraction is always substantially larger than the fraction of significantly responsive Purkinje cells, indicating a tendency of similar Purkinje cells to group together. Statistical significance was tested by comparing the fraction of Purkinje cells with statistically significant responses and the fraction of neighbours of Purkinje cells with statistically significant responses that showed statistically significant responses as well (after correction for border effects) using Fisher's exact test and after Benjamini-Hochberg correction for multiple comparisons: * $p < 0.05$; *** $p < 0.001$.

Figure 7 – Purkinje cell responses to single whisker stimulation show weak clustering
(A) To investigate smaller receptive fields, we sequentially stimulated five of the large facial whiskers. To avoid interference with other whiskers during active movement, we performed these experiments under ketamine/xylazine anaesthesia. Most Purkinje cells, if responsive to single-whisker stimulation, responded only to one of the five whiskers **(B)**. This is illustrated by five peri-stimulus time histograms (PSTHs) from a single, representative Purkinje cell. This particular cell was sensitive to stimulation of the C3 whisker only. The average and 3 s.d. of the baseline firing are indicated (dashed line and grey area). **(C)** Purkinje cells that responded to more than one whisker were typically responsive to the more anterior whiskers (see also Table 5). The widths of the lines indicate the Z value of the occurrence of multiple responses per cell. **(D)** Two recording spots, in close proximity in crus 1 of the same animal,

with the identified Purkinje cell dendritic trees. For each dendrite, the colour indicates the whisker(s) to which it was responsive (see legend below with grey denoting the absence of a statistically significant response). **(E)** For each of the two recording sites, the average of the responsive and the non-responsive Purkinje cells is indicated (to the C3 whisker in the left panel and to the C2 whisker in the right panel). Note that only a single cell was responsive to C2 stimulation in recording spot 2. The shades indicate inter-quartile ranges. **(F)** Linear regression revealed that Purkinje cells that were surrounded by other Purkinje cells responsive to the same whisker (same colour code as in **A**) had a tendency to show stronger responses to stimulation of that whisker than Purkinje cells that were more isolated. The x-axis represents the fraction of Purkinje cells responsive to the particular whisker within the respective field of view. $R = 0.521$; $p < 0.001$.

Figure 8 – Purkinje cells encoding the same response group together

(A) Representative field of view with Purkinje cell dendrites. Purkinje cells showing statistically significant responses to whisker pad stimulation are depicted in shades of red and the other cells in shades of blue. **(B)** For each pair of Purkinje cells we calculated the Pearson correlation coefficient (R) during 1 Hz whisker pad stimulation. The pairs of two Purkinje cells that were both statistically significantly responsive to whisker pad stimulation (red symbols) had on average a higher level of synchrony than the pairs connecting a responsive and a non-responsive Purkinje cell (grey symbols; $p < 0.001$; two-dimensional Kolmogorov-Smirnov test). The pairs consisting of two non-responsive Purkinje cells were excluded from this analysis. **(C)** Interestingly, even in the absence of sensory stimulation, the pairs of Purkinje cells that were both responsive to whisker pad stimulation maintained a higher level of synchrony than “heterogeneous pairs”. Thus, Purkinje cells with the same receptive field tended to fire more synchronously, even in the absence of stimulation. This analysis was expanded in the presence **(D)** and absence **(E)** of sensory stimulation for six different types of stimulation and illustrated as the median R value per distance category (six bin values of equal distance at a log scale). The shaded areas represent the inter-quartile ranges. * $p < 0.05$; *** $p < 0.001$ (two-dimensional Kolmogorov-Smirnov tests after Benjamini-Hochberg correction).

Figure 9 – Purkinje cells encode strong and weak sensory stimulation via synchronous firing

(A) Aggregate peri-stimulus time histograms (PSTHs) show that coherent firing of complex spikes predominantly occurs following sensory stimulation. For each field of view, we calculated the number of complex spikes occurring per frame, summing those of all Purkinje cells in that field of view. Subsequently, we made aggregate PSTHs where the colour of each bin refers to the number of dendrites simultaneously active. In this field of view, 17 Purkinje cells were measured. Of these, 17 (100%) reacted to air puff, 12 (71%) to whisker pad, 3 (18%) to upper lip, 4 (24%) to lower lip and 1 (6%) to cheek stimulation. **(B)** Based upon a Poisson distribution of complex spikes over all dendrites and bins, one would expect between 0 and 3 simultaneously active dendrites (grey bars). The red bars indicate events involving more dendrites simultaneously than expected from a random distribution. Thus, the sparse firing as expected by chance is relatively constant throughout the trials, but the simultaneous activity of multiple dendrites is strongly enhanced following sensory stimulation. **(C)** A direct overlay of the aggregate PSTHs in response to air puff and lower lip stimulation shows that the strong response found after air puff stimulation comes at the expense of inter-trial complex spikes (152 trials per condition). **(D)** For equally long recordings in the presence of different types of stimulation, equal complex spike frequencies were observed as during spontaneous activity ($F(2.544, 20.348) = 2.561$, $p = 0.091$, repeated measures ANOVA), indicating that sensory stimulation results in a temporal re-ordering of complex spikes, rather than to the production of more complex spikes.

Figure 10 – Sensory stimulation results in a temporal re-ordering of complex spikes

(A) The temporal distribution of complex spikes was compared in a pairwise fashion between sessions with sensory stimulation and sessions without. For this analysis, we included only Purkinje cells that displayed a statistically significant response to the stimulus involved (n = 102 for air puff, n = 45 for whisker pad and n = 27 for visual stimulation). The spontaneous recordings were analyzed by creating post hoc pseudo-stimuli at the same 1 Hz frequency as during sensory stimulation. Shown are the medians of the peri-stimulus time histograms. The shaded areas indicate the inter-quartile ranges. **(B)** The reduction in baseline firing, measured during the -500 to -250 ms interval, was significant in all cases (Wilcoxon matched-pairs test after Benjamini-Hochberg correction for multiple comparisons). **(C)** The larger the response amplitude, the stronger the reduction in inter-trial firing (Pearson correlation tests after Benjamini-Hochberg correction for multiple comparisons). This analysis was performed on

all Purkinje cells (n = 117 for air puff and whisker pad stimulation and n = 60 for LED stimulation; dotted lines mark the criterion for statistical significance at Z = 3). Note the differences in the x-axis scaling with the air puff evoking relatively stronger responses. * p < 0.05; *** p < 0.001

Supporting information

Figure S1 - Complex spike detection

Figure S2 – Purkinje cells in crus 1 respond to various types of sensory stimulation

Figure S3 – Sound only stimulation systematically recruited less complex spikes than tactile stimulation

Figure S4 – Stimulus strength has only a minor impact on complex spike responsiveness

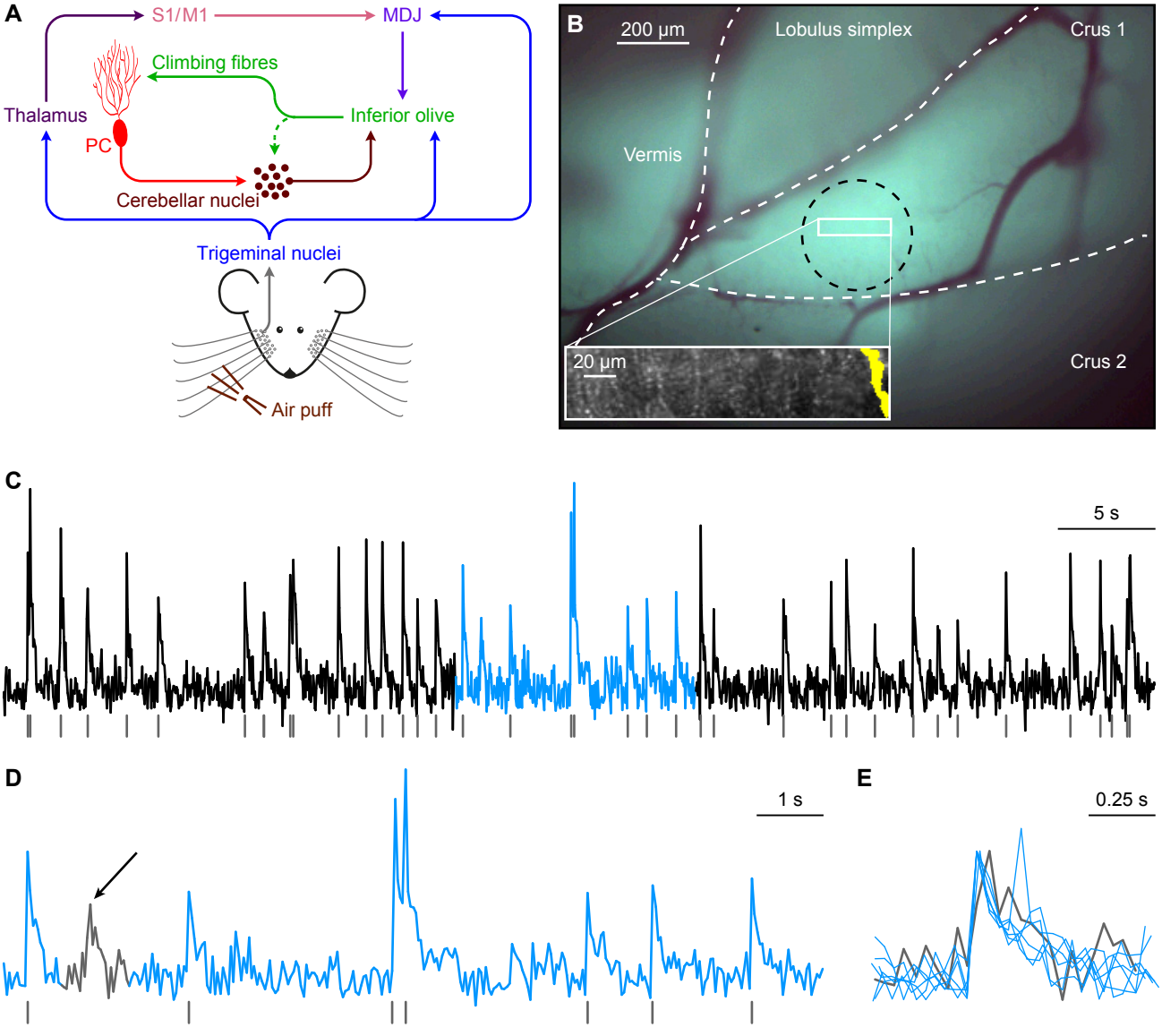

Figure 1 – Sensory pathways carrying facial input to the cerebellar cortex

(A) Scheme of the main routes conveying facial tactile input via the climbing fibre pathway to cerebellar Purkinje cells (PC). Climbing fibres, which cause complex spike firing in Purkinje cells, exclusively originate from the inferior olive. The inferior olive, in turn, is directly innervated by neurons from the trigeminal nuclei as well as indirectly via thalamo-cortical pathways that project to the inferior olive mainly via the nuclei of the mesodiencephalic junction (MDJ). The MDJ itself also receives direct input from the trigeminal nuclei. See the main text for references. **(B)** *In vivo* two-photon Ca^{2+} imaging was performed to characterize Purkinje cell complex spike responses to sensory stimulation in the medial part of crus 1. Purkinje cells were detected using independent component analysis and the position of a Purkinje cell dendrite (yellow area on the right) within a field of view is shown in the inset. At the end of each recording session, the brain was removed and the location of the dye injection in medial crus 1 was confirmed through *ex vivo* epifluorescent imaging (black circle). The white rectangle indicates the approximate recording location. **(C)** Complex spikes that were triggered by climbing fibre activity were retrieved from fluorescent traces of individual Purkinje cells. A representative trace obtained from the Purkinje cell dendrite illustrated in **B** is shown together with the detected complex spikes (grey lines). The light blue episode is enlarged in **D**. Complex spikes were detected by the combination of a threshold and a template matching algorithm. Only events with a sharp rising phase were accepted as complex spikes. In the 60 s interval shown in **C**, there was one event with a slower rise time (see arrow in **D**), as indicated at a larger time scale in **E**. The events in **E** are scaled to peak.

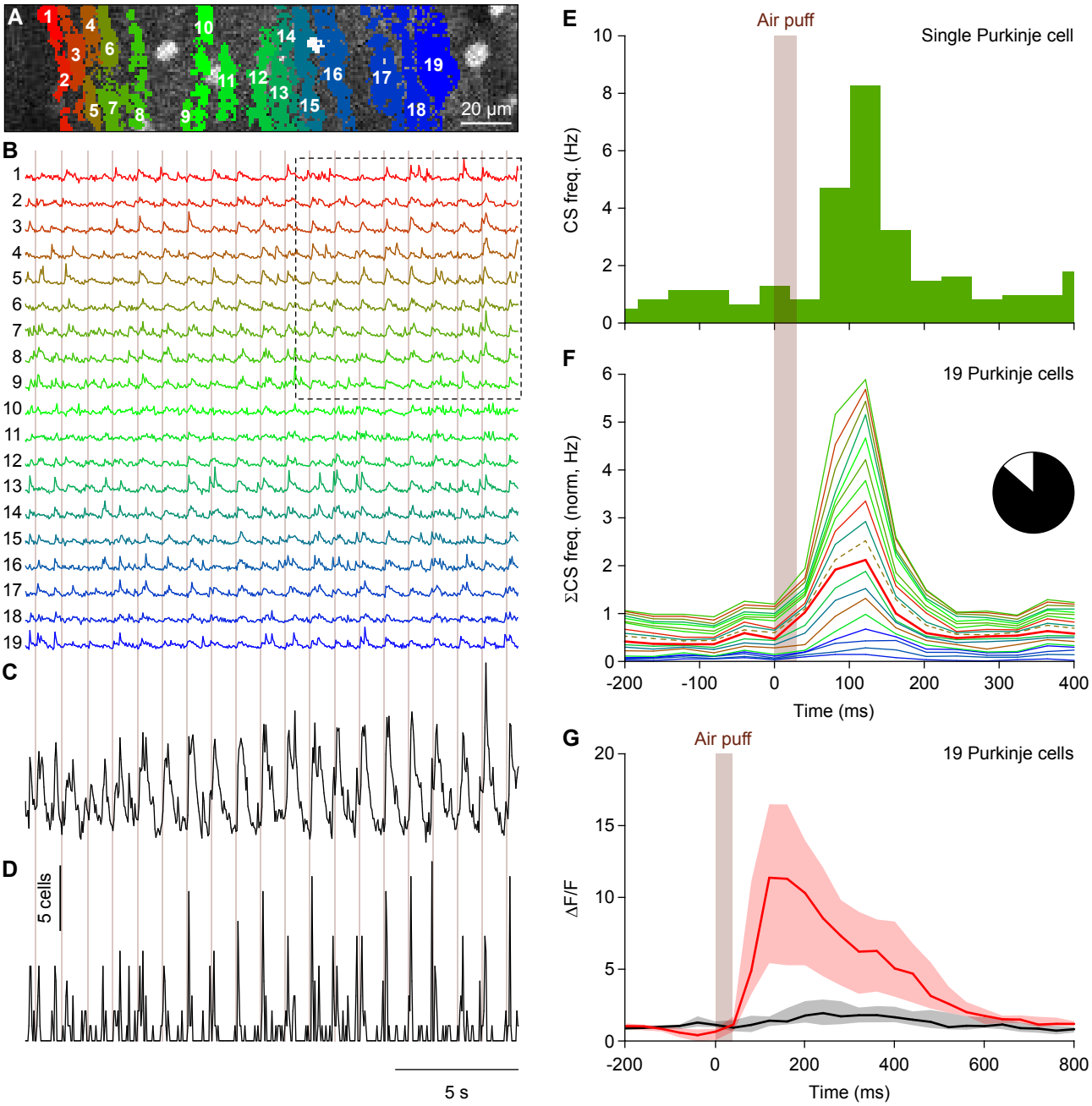

Figure 2 - Whisker stimulation evokes complex spike responses in cerebellar crus 1

(A) Complex spikes elicit large increases in the Ca^{2+} concentration within Purkinje cell dendrites that can be resolved using *in vivo* two-photon microscopy in combination with a fluorescent Ca^{2+} indicator. An example of a field of view with 19 identified Purkinje cell dendrites located in the medial part of crus 1 is shown with each individual dendrite denoted by a number and a unique colour. This recording was made in an awake mouse. **(B)** The fluorescent traces of each of these dendrites show distinct Ca^{2+} transient events, which are to a large extent associated with air puff stimulation of the facial whiskers (times of stimulation indicated by the vertical lines). The boxed area is enlarged in Fig. S1. **(C)** Summed fluorescence trace composed of all 19 individual traces emphasizing the participation of many Purkinje cells to the stimulus-triggered responses. **(D)** After complex spike extraction, a clear relation between stimulus and activity was observed as illustrated by summing, for each frame, the number of complex spikes observed over all dendrites. The vertical scale bar corresponds to the simultaneous activity of 5 Purkinje cells. **(E)** Peri-stimulus time histogram of a Purkinje cell dendrite (marked as number 7 in **A** and **B**) in response to air puff stimulation to the ipsilateral whiskers (154 trials). The bin size (40 ms) corresponds to the acquisition frame rate (25 Hz). **(F)** Normalized stacked line graph of the Purkinje cells in this field of view showing that every cell contributed to the overall response. The Purkinje cells are ranked by their maximal response and the data are normalized so that the top line reflects the average frequency per bin. Cell no. 7 (dashed line) had a relatively poor signal-to-noise ratio during later parts of the recording (see Fig. S1), but it had nevertheless a complex spike response profile that was indistinguishable from the other cells. The colours match those in the panels **A**-**B**. Inset: In total, 102 out of 117 cells analysed (87%) were responsive to whisker air puff stimulation (peak response exceeded average + 3 s.d. of pre-stimulus interval). **(G)** Fluorescent traces of the trials with (red) and without (black) complex spikes fired during the first 200 ms after air puff onset. In the absence of complex spike firing, only a very small increase in fluorescence was observed, indicating that the majority of change in fluorescence was associated with complex spike firing. Note the longer time scale than in **E** and **F**. The lines indicate the medians and the shaded areas the inter-quartile ranges of the 19 Purkinje cells in this field of view.

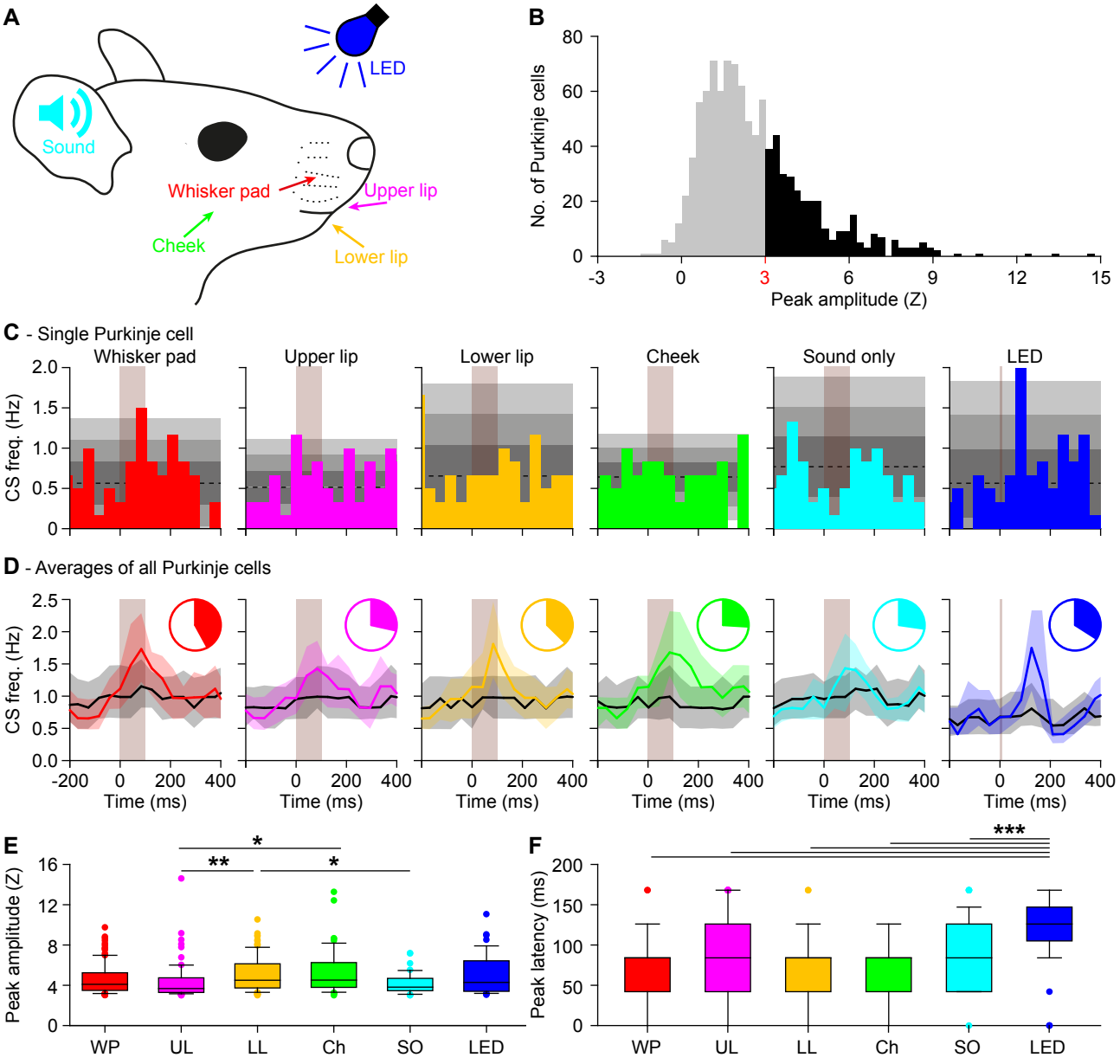

Figure 3 – Purkinje cells in crus 1 respond to various types of sensory stimulation

(A) Tactile stimuli were presented to four facial regions in awake mice: the whisker pad (WP), the upper lip (UL), the lower lip (LL) and the cheek (Ch). Each stimulus was delivered with a piezo-actuator that made a muted, yet audible sound which was also delivered without touch ("sound only (SO)"). A blue light flash generated by an LED was used as visual stimulus. These experiments were performed in awake mice. **(B)** To avoid interference of adjacent areas, we applied gentle touches (0.686 mN). The complex spike response ratio was much reduced relative to the strong air puff stimulation to all ipsilateral whiskers illustrated in Fig. 2. A histogram of the peak responses (expressed as Z value) of all responses to either of the four tactile stimuli demonstrates that the response strength is a continuum, showing the lack of a clear separation between "responsive" and "non-responsive" Purkinje cells (998 stimulus conditions in 282 Purkinje cells). We considered Purkinje cells that showed a peak response above Z = 3 as "significantly responsive" (represented with black bars), but we provide most of the analyses also for the population as a whole (e.g., Fig. S2). **(C)** The peri-stimulus time histograms (PSTHs) of a representative Purkinje cell. The shades of grey indicate 1, 2 and 3 s.d. around the average. Each stimulus was repeated 154 times at 1 Hz. **(D)** For every stimulus condition, we averaged the PSTHs for all Purkinje cells that were significantly responsive to that particular stimulus (coloured lines; medians (inter-quartile range)). These were contrasted to the averaged PSTH of the other Purkinje cells (black lines). The pie charts represent the fraction of Purkinje cells significantly responsive to a particular stimulus. See also Table 1. **(E)** The peak responses of the significantly responding Purkinje cells were the lowest for sound only and for upper lip stimulation. * $p < 0.05$; ** $p < 0.01$ (post-hoc tests after Kruskal-Wallis test) **(F)** As expected for complex spike responses to weak stimulation, the latencies were relatively long and variable, but consistent across types of stimulation. Only visual stimulation (LED) had a remarkably longer latency time. *** $p < 0.001$ (post-hoc tests after Kruskal-Wallis test for LED vs. whisker pad, upper lip, lower lip and cheek and $p < 0.05$ compared to sound only)

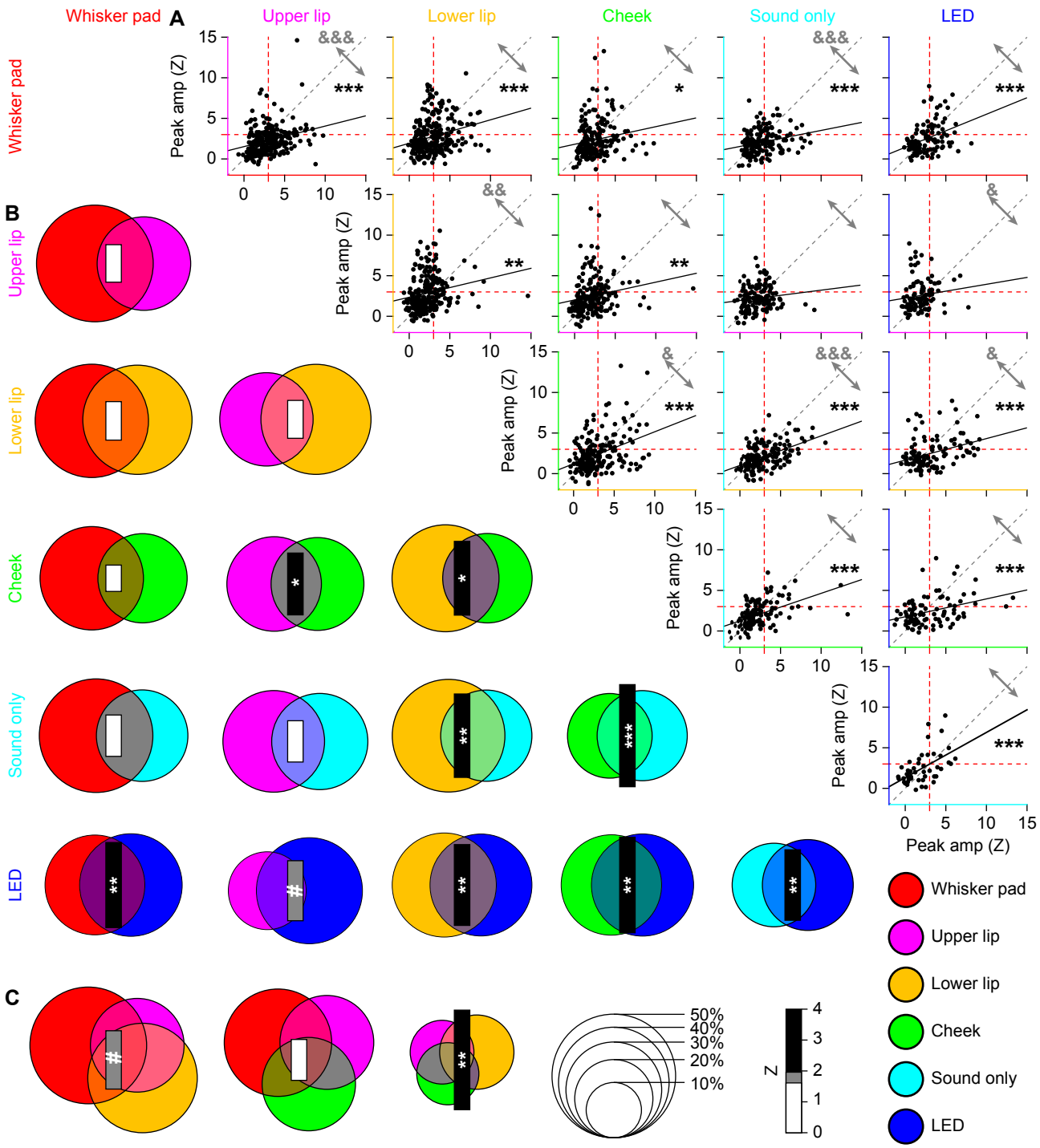

Figure 4 – Convergence of sensory input on Purkinje cells
(A) In order to test whether sensory inputs converge on individual Purkinje cells in awake mice, we made pair-wise comparisons of the response amplitudes to two different stimuli per Purkinje cell (scatter plots). For all possible combinations, we found a positive slope of the linear regression analysis. For the majority of combinations, the correlation between response strengths was highly significant: * $p < 0.05$, ** $p < 0.01$ and *** $p < 0.001$ (Pearson correlation with Benjamini-Hochberg correction for multiple comparisons). Only upper lip vs. sound only and upper lip vs. visual stimulation were not significantly correlated. For this analysis, we included all Purkinje cells, whether they had a statistically significant response or not. The red dotted lines indicate a Z-score of 3, which we set as the threshold for significance (cf. Fig. 3B). They grey arrows indicate the fraction of observations above and below the unity line (grey dotted line). The relative strengths of every stimulus combination were compared in a pairwise fashion (Wilcoxon tests with Benjamini-Hochberg correction for multiple comparisons): & $p < 0.05$; && $p < 0.01$; &&& $p < 0.001$. **(B)** We performed a similar analysis focusing only on statistically significant responses (Venn diagrams). Again, all combinations had a positive Z score (as evaluated by a bootstrap method; see Methods), indicating more than expected convergence. The diameter of each circle indicates the fraction of Purkinje cells showing a significant response to that particular, colour coded stimulus. The size of the bar represents the Z score of the overlapping fraction. **(C)** The same for the combinations of three tactile stimuli. Overall, sensory streams tended to converge, rather than diverge, on Purkinje cells. # $p < 0.10$; * $p < 0.05$, ** $p < 0.01$ and *** $p < 0.001$ (Z test with Benjamini-Hochberg correction).

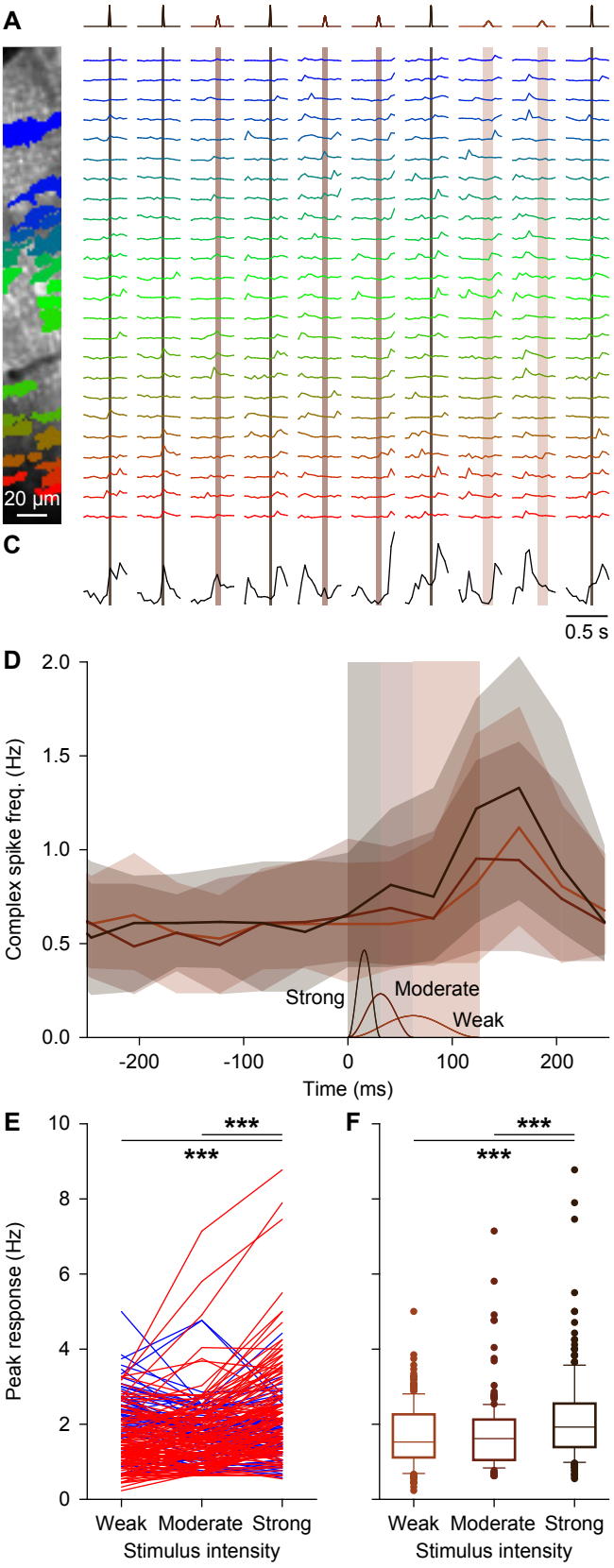

Figure 5 – Stimulus strength has only a minor impact on complex spike responsiveness

(A) Movements of all large facial whiskers were performed using a piezo-actuator at three different speeds (weak: 1 mm displacement in 62 ms; moderate: 2 mm displacement in 31 ms; strong: 4 mm displacement in 16 ms). The stimulus sequence was randomly permuted. The recordings were made in awake mice. **(B)** Field of view with 24 identified and colour-coded Purkinje cells (left) and their corresponding fluorescent traces (right). Stimuli were presented every 2 s and in between trials the laser illumination was briefly blocked to avoid photobleaching. Note that the periods without laser illumination are not drawn to scale. The vertical shaded areas indicate stimulus duration (which was inverse with the stimulus strength). **(C)** Summed fluorescence trace composed of all 24 individual traces showing that not all trials evoked ensemble-wide responses. Some spontaneous, inter-trial activity was also observed. **(D)** The median number of complex spikes per frame (of 40 ms) per trial (shaded areas: inter-quartile range) for the three stimulus strengths show little difference for the weak and moderate stimulation. The time course and amplitude (1-4 mm) of the three stimuli is schematized at the bottom of the graph. Strong stimulation elicited about 30% more complex spikes, as evident from the peak responses for each stimulus intensity. **(E)** Plotting for each of Purkinje cell the average peak response for each stimulus condition results in many overlapping lines. Only a few cells stand out in that they show a strong response that consistently increases with stimulus strength (red lines on top). The Purkinje cells that showed increased responsiveness to stronger stimuli are depicted in red and the others in blue (see also Fig. S4A). **(F)** The same data summarized with box plots for all significantly responsive cells. Data are from 209 significantly responsive Purkinje cells (out of 340 Purkinje cells that were measured in this way). *** $p < 0.001$ (Friedman's test).

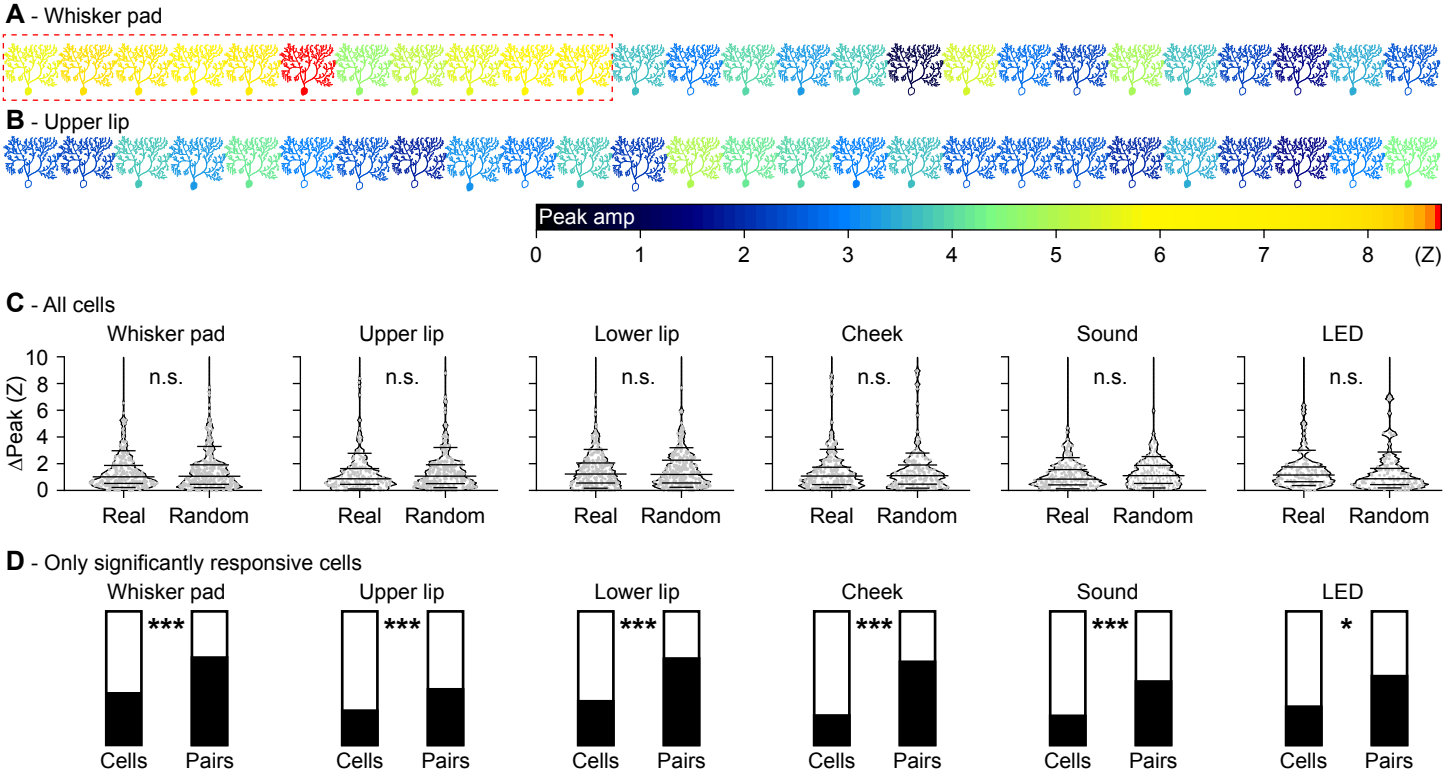

Figure 6 - Purkinje cells encoding the same stimulus have a tendency to be spatially grouped

Schematic drawing of a field of view with 26 Purkinje cells organized in the medio-lateral direction of crus 1 in an awake mouse. The colour of each Purkinje cell corresponds to the maximal response to whisker pad **(A)** or upper lip **(B)** stimulation. Purkinje cells with a filled soma had a peak response with a Z score > 3 and were considered to be statistically significant, in contrast to those with an open soma. Responsive and non-responsive cells are generally intermingled, but a group of "strong responders" can be observed for whisker pad stimulation (red rectangle). **(C)** The anecdotal data in **A** suggest the presence of clusters of Purkinje cells encoding specific stimuli. For this to be the case, one would expect that neighbouring Purkinje cells have roughly similar response strengths. We found that this assumption does not hold as the differences in response strengths of neighbours could not be discriminated from randomly selected cells in the same recording if all Purkinje cells are considered (compared with bootstrap analysis based upon randomly chosen cell pairs within each field of view: all $p > 0.8$; Z test). Data are represented in violin plots, with the grey lines indicating the 10th, 25th, 50th, 75th and 90th percentiles. **(D)** When considering only the Purkinje cells with statistically significant responses, spatial grouping does occur. For each stimulus type, the black portion of the left bar indicates the fraction of Purkinje cells showing a significant response to that stimulus. The filled portion of the right bar indicates the fraction of the neighbours (always on the medial side) of these significantly responsive Purkinje cells that were also significantly responsive. As can be seen, this fraction is always substantially larger than the fraction of significantly responsive Purkinje cells, indicating a tendency of similar Purkinje cells to group together. Statistical significance was tested by comparing the fraction of Purkinje cells with statistically significant responses and the fraction of neighbours of Purkinje cells with statistically significant responses that showed statistically significant responses as well (after correction for border effects) using Fisher's exact test and after Benjamini-Hochberg correction for multiple comparisons: * $p < 0.05$; *** $p < 0.001$.

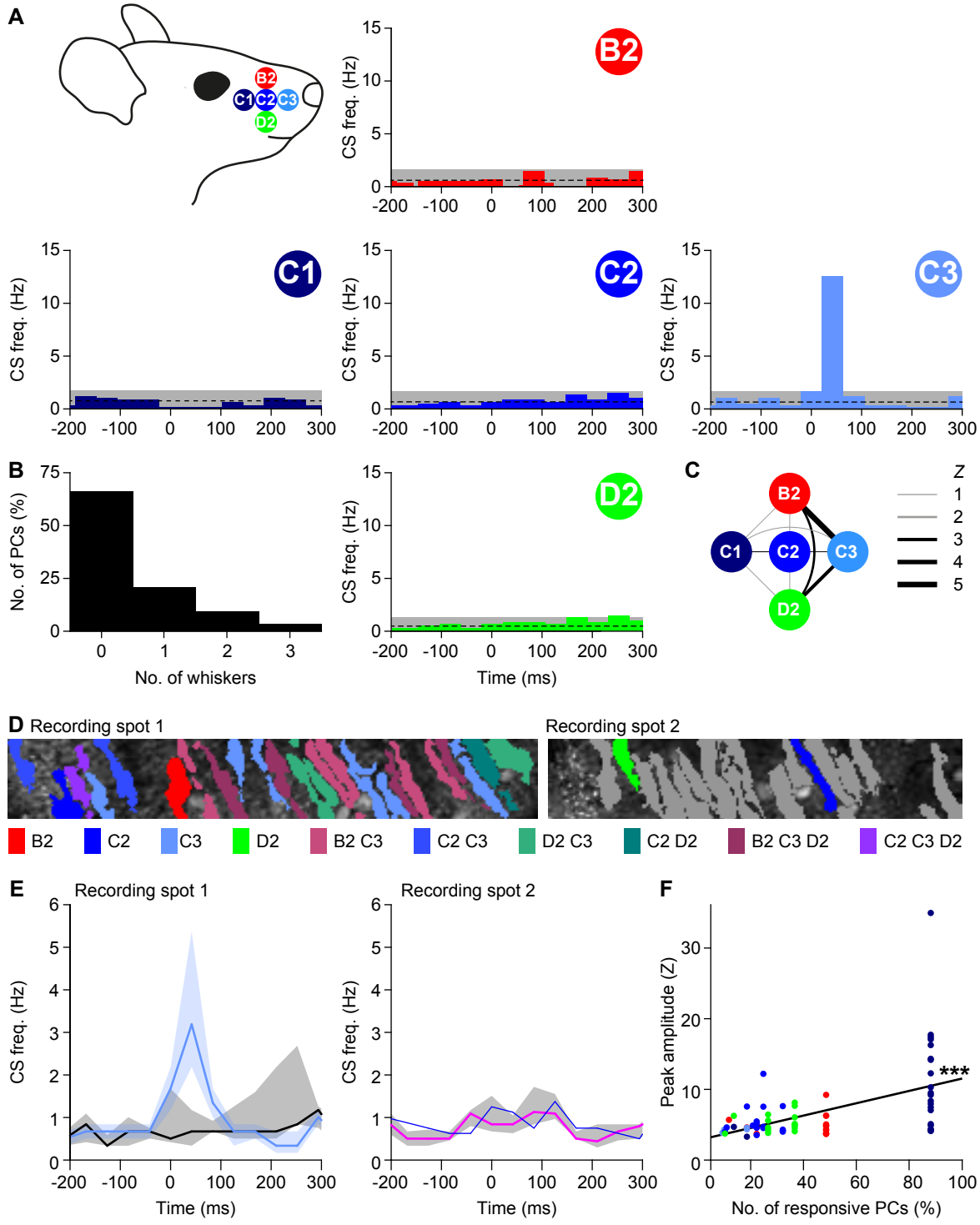

Figure 7 – Purkinje cell responses to single whisker stimulation show weak clustering

(A) To investigate smaller receptive fields, we sequentially stimulated five of the large facial whiskers. To avoid interference with other whiskers during active movement, we performed these experiments under ketamine/xylazine anesthesia. Most Purkinje cells, if responsive to single-whisker stimulation, responded only to one of the five whiskers **(B)**. This is illustrated by five peri-stimulus time histograms (PSTHs) from a single, representative Purkinje cell. This particular cell was sensitive to stimulation of the C3 whisker only. The average and 3 s.d. of the baseline firing are indicated (dashed line and grey area). **(C)** Purkinje cells that responded to more than one whisker were typically responsive to the more anterior whiskers (see also Table 5). The widths of the lines indicate the Z value of the occurrence of multiple responses per cell. **(D)** Two recording spots, in close proximity in crus 1 of the same animal, with the identified Purkinje cell dendritic trees. For each dendrite, the colour indicates the whisker(s) to which it was responsive (see legend below with grey denoting the absence of a statistically significant response). **(E)** For each of the two recording sites, the medians of the responsive and the non-responsive Purkinje cells are indicated (to the C3 whisker in the left panel and to the C2 whisker in the right panel). Note that only a single cell was responsive to C2 stimulation in recording spot 2. The shades indicate inter-quartile ranges. **(F)** Linear regression revealed that Purkinje cells that were surrounded by other Purkinje cells responsive to the same whisker (same colour code as in **A**) had a tendency to show stronger responses to stimulation of that whisker than Purkinje cells that were more isolated. The x-axis represents the fraction of Purkinje cells responsive to the particular whisker within the respective field of view. R = 0.521; $p < 0.001$.

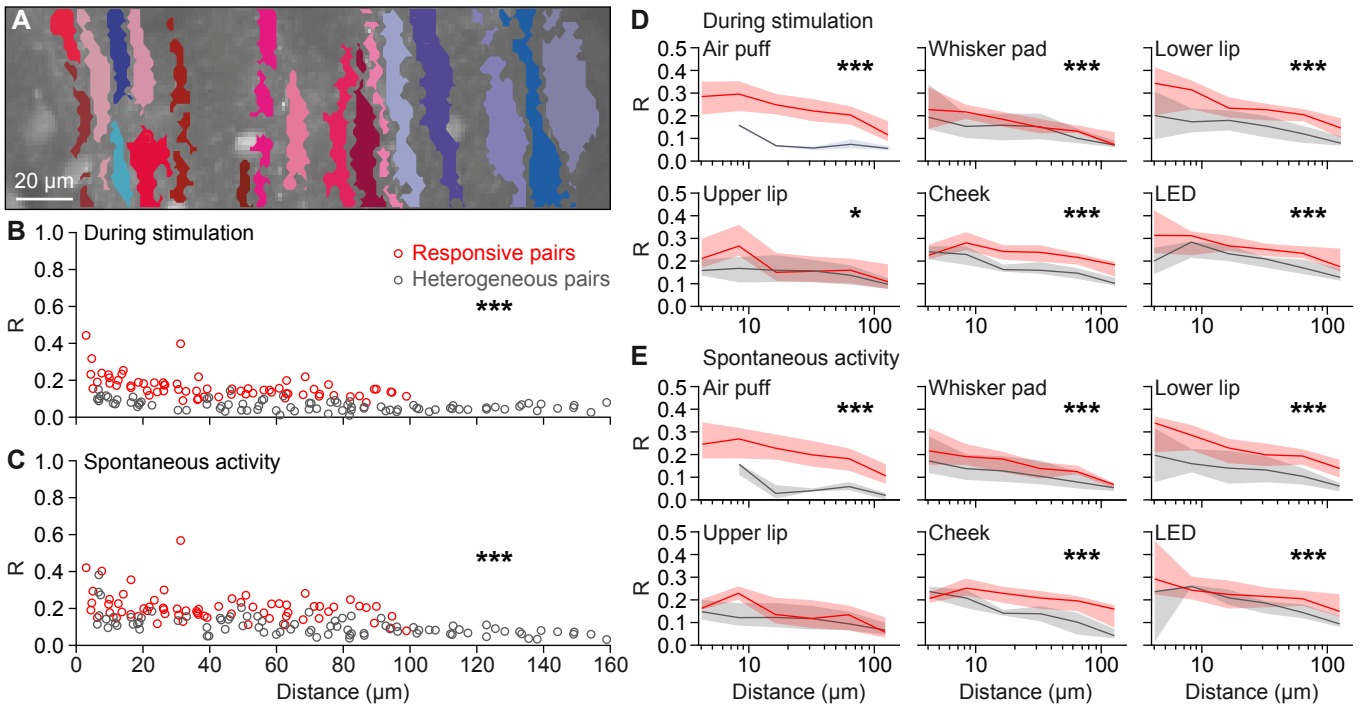

Figure 8 – Purkinje cells encoding the same response group together

(A) Representative field of view with Purkinje cell dendrites. Purkinje cells showing statistically significant responses to whisker pad stimulation are depicted in shades of red and the other cells in shades of blue. **(B)** For each pair of Purkinje cells we calculated the Pearson correlation coefficient (R) during 1 Hz whisker pad stimulation. The pairs of two Purkinje cells that were both statistically significantly responsive to whisker pad stimulation (red symbols) had on average a higher level of synchrony than the pairs connecting a responsive and a non-responsive Purkinje cell (grey symbols; $p < 0.001$; two-dimensional Kolmogorov-Smirnov test). The pairs consisting of two non-responsive Purkinje cells were excluded from this analysis. **(C)** Interestingly, even in the absence of sensory stimulation, the pairs of Purkinje cells that were both responsive to whisker pad stimulation maintained a higher level of synchrony than "heterogeneous pairs". Thus, Purkinje cells with the same receptive field tended to fire more synchronously, even in the absence of stimulation. This analysis was expanded in the presence **(D)** and absence **(E)** of sensory stimulation for six different types of stimulation and illustrated as the median R value per distance category (six bin values of equal distance at a log scale). The shaded areas represent the inter-quartile ranges. * $p < 0.05$; *** $p < 0.001$ (two-dimensional Kolmogorov-Smirnov tests after Benjamini-Hochberg correction).

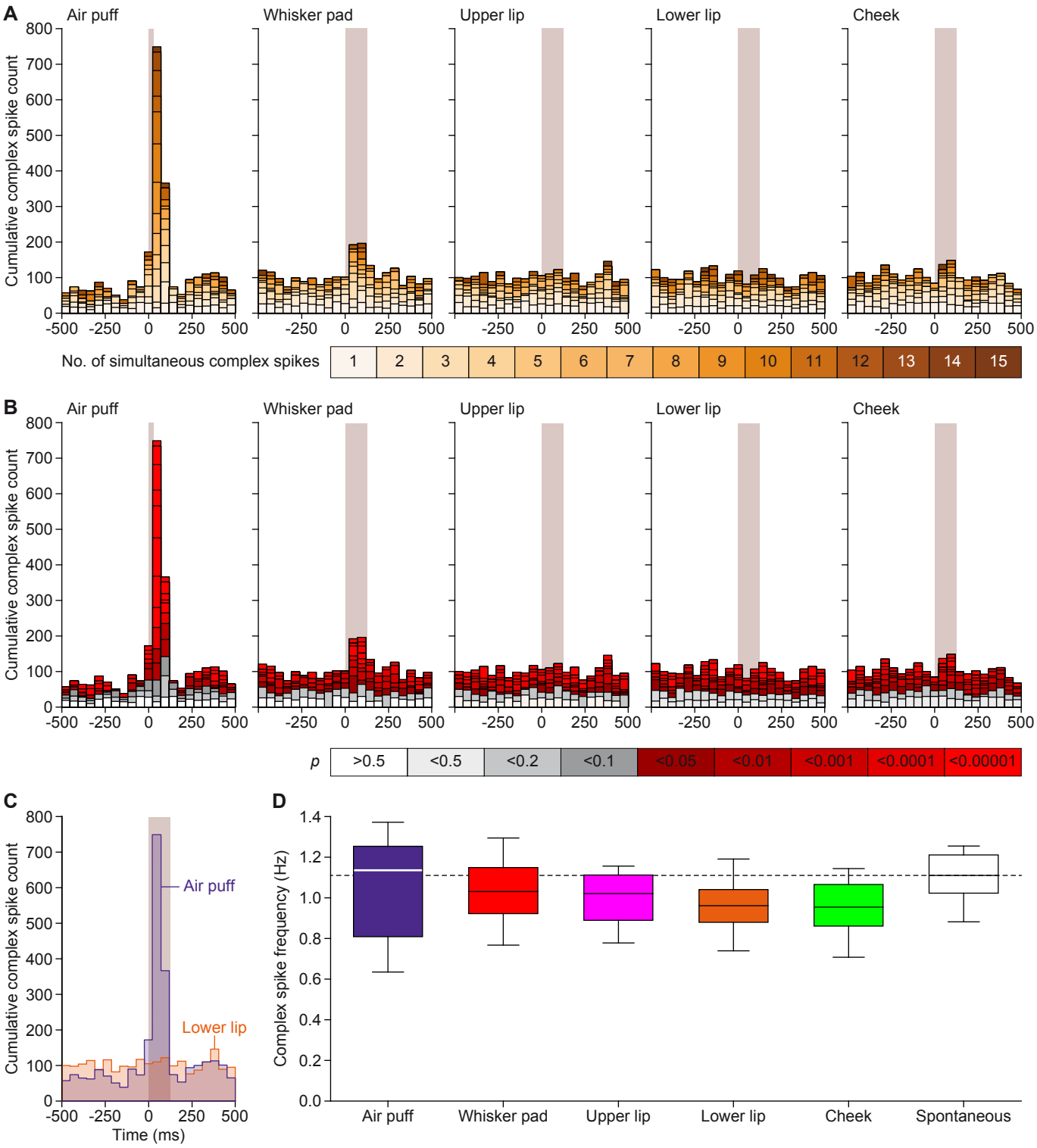

Figure 9 – Purkinje cells encode strong and weak sensory stimulation via synchronous firing

(A) Aggregate peri-stimulus time histograms (PSTHs) show that coherent firing of complex spikes predominantly occurs following sensory stimulation. For each field of view, we calculated the number of complex spikes occurring per frame, summing those of all Purkinje cells in that field of view. Subsequently, we made aggregate PSTHs where the colour of each bin refers to the number of dendrites simultaneously active. In this field of view, 17 Purkinje cells were measured. Of these, 17 (100%) reacted to air puff, 12 (71%) to whisker pad, 3 (18%) to upper lip, 4 (24%) to lower lip and 1 (6%) to cheek stimulation. **(B)** Based upon a Poisson distribution of complex spikes over all dendrites and bins, one would expect between 0 and 3 simultaneously active dendrites (grey bars). The red bars indicate events involving more dendrites simultaneously than expected from a random distribution. Thus, the sparse firing as expected by chance is relatively constant throughout the trials, but the simultaneous activity of multiple dendrites is strongly enhanced following sensory stimulation. **(C)** A direct overlay of the aggregate PSTHs in response to air puff and lower lip stimulation shows that the strong response found after air puff stimulation comes at the expense of intertrial complex spikes (152 trials per condition). **(D)** For equally long recordings in the presence of different types of stimulation, equal complex spike frequencies were observed as during spontaneous activity ($F(2.544, 20.348) = 2.561$, $p = 0.091$, repeated measures ANOVA), indicating that sensory stimulation results in a temporal re-ordering of complex spikes, rather than to the production of more complex spikes.

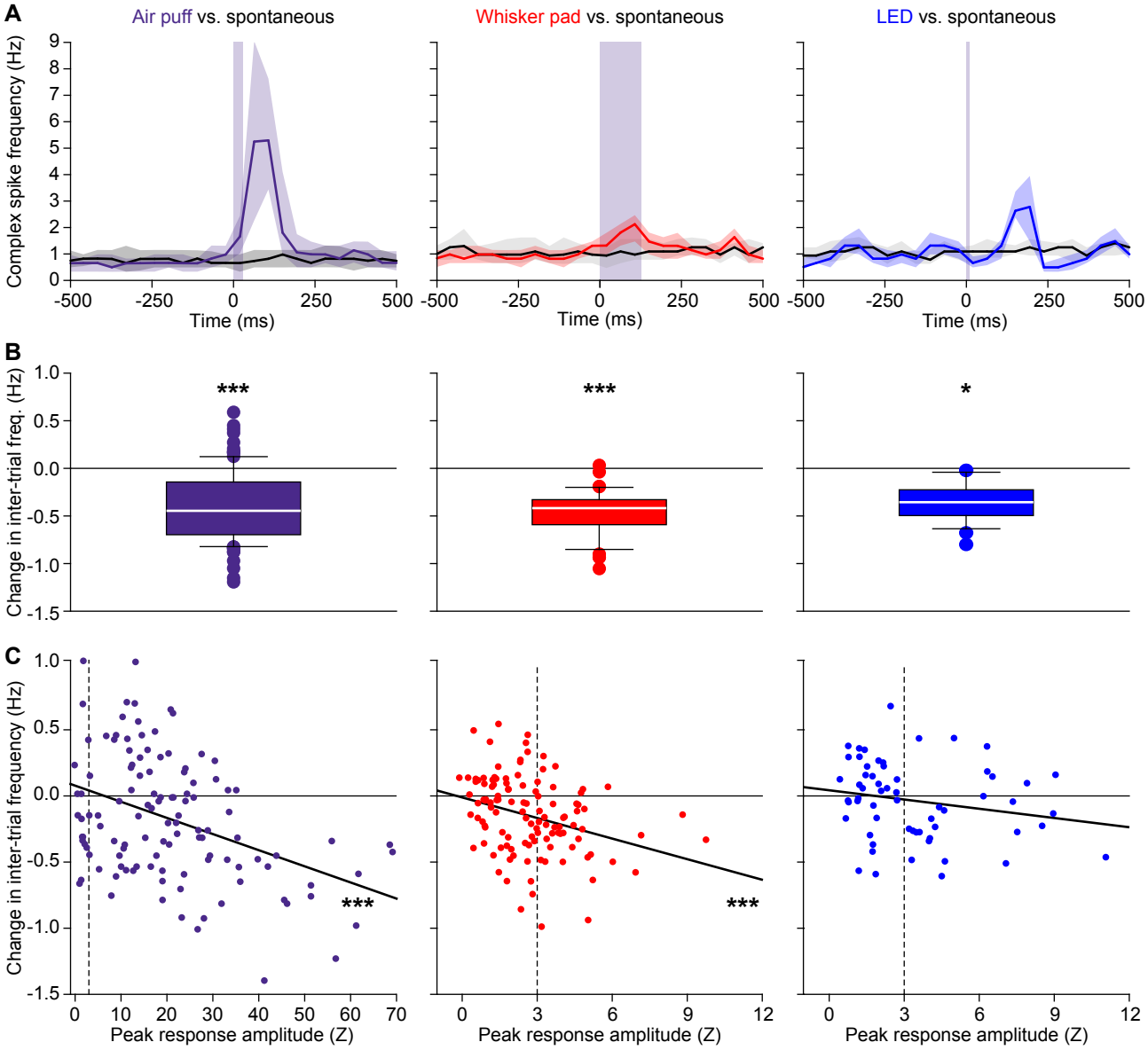

Figure 10 – Sensory stimulation results in a temporal re-ordering of complex spikes
(A) The temporal distribution of complex spikes was compared in a pairwise fashion between sessions with sensory stimulation and sessions without. For this analysis, we included only Purkinje cells that displayed a statistically significant response to the stimulus involved (n = 102 for air puff, n = 45 for whisker pad and n = 27 for visual stimulation). The spontaneous recordings were analyzed by creating *post hoc* pseudo-stimuli at the same 1 Hz frequency as during sensory stimulation. Shown are the medians of the peri-stimulus time histograms. The shaded areas indicate the inter-quartile ranges. **(B)** The reduction in baseline firing, measured during the -500 to -250 ms interval, was significant in all cases (Wilcoxon matched-pairs test after Benjamini-Hochberg correction for multiple comparisons). **(C)** The larger the response amplitude, the stronger the reduction in inter-trial firing (Pearson correlation tests after Benjamini-Hochberg correction for multiple comparisons). This analysis was performed on all Purkinje cells (n = 117 for air puff and whisker pad stimulation and n = 60 for LED stimulation; dotted lines mark the criterion for statistical significance at Z = 3). Note the differences in the x-axis scaling with the air puff evoking relatively stronger responses. * $p < 0.05$; *** $p \leq 0.001$